

### **OPEN ACCESS**

EDITED BY Robert Fruscio, University of Milano Bicocca, Italy

REVIEWED BY
Francesco Ricchetti,
Sacro Cuore Don Calabria
Hospital (IRCCS), Italy
Yi Zhu,
Sichuan Cancer Hospital, China

\*CORRESPONDENCE
Ji Wu

☑ gxnnwuji@163.com

RECEIVED 06 August 2025 ACCEPTED 27 October 2025 PUBLISHED 13 November 2025

### CITATION

Wang J, Bao S, Huang T, Cai Y, Jin B and Wu J (2025) Fusion model combining ultrasound-based radiomics and deep transfer learning with clinical parameters for preoperative prediction of pelvic lymph node metastasis in cervical cancer. *Front. Oncol.* 15:1681029. doi: 10.3389/fonc.2025.1681029

### COPYRIGHT

© 2025 Wang, Bao, Huang, Cai, Jin and Wu. This is an open-access article distributed under the terms of the Creative Commons Attribution License (CC BY). The use, distribution or reproduction in other forums is permitted, provided the original author(s) and the copyright owner(s) are credited and that the original publication in this journal is cited, in accordance with accepted academic practice. No use, distribution or reproduction is permitted which does not comply with these terms.

# Fusion model combining ultrasound-based radiomics and deep transfer learning with clinical parameters for preoperative prediction of pelvic lymph node metastasis in cervical cancer

Jihan Wang<sup>1</sup>, Shengxian Bao<sup>2</sup>, Tongtong Huang<sup>1</sup>, Yongzhi Cai<sup>1</sup>, Binbin Jin<sup>1</sup> and Ji Wu<sup>1\*</sup>

<sup>1</sup>Department of Ultrasonic Medicine, the First Affiliated Hospital of Guangxi Medical University, Nanning, Guangxi, China, <sup>2</sup>Department of Ultrasonic Medicine, the Affiliated Tumor Hospital of Guangxi Medical University, Nanning, Guangxi, China

**Background:** To develop and validate a multimodal fusion model integrating ultrasound-based radiomics, deep transfer learning (DTL), and clinical parameters for preoperative pelvic lymph node metastasis (PLNM) prediction in cervical cancer.

**Methods:** A retrospective cohort of 421 patients with surgically confirmed cervical cancer was divided into the training (70%, n = 294) and testing (30%, n = 127) sets. Ultrasound-based radiomics (1,561 handcrafted features) and 3 DTL architectures (DenseNet121, ResNet50, AlexNet) were employed for feature extraction. After redundancy reduction (Spearman correlation, least absolute shrinkage and selection operator regression) and principal component analysis, fused radiomics-DTL features were combined with clinical predictors. Eight machine learning classifiers were evaluated, and the optimal model was used to construct a nomogram. Performance was assessed using area under the curve (AUC), calibration curves, and decision curve analysis (DCA).

**Results:** The multilayer perceptron-based fusion model achieved a testing AUC of 0.753, outperforming standalone radiomics (AUC = 0.729) and DTL models (best AUC = 0.702; DenseNet121). Integration of clinical predictors (maximum tumor diameter and red blood cell count) further enhanced performance, yielding a nomogram with training/testing AUCs of 0.871 and 0.764, and a testing sensitivity and specificity of 58.1% and 84.4%,respectively. DCA demonstrated superior clinical utility for the nomogram across threshold probabilities (10%-50%).

**Conclusions:** We developed a multimodal fusion model integrating ultrasound-based radiomics, DTL, and clinical parameters for preoperative PLNM prediction in cervical cancer. The proposed nomogram provides a clinically applicable, cost-effective tool for preoperative PLNM prediction, particularly valuable for optimizing treatment decisions in resource-limited settings.

KEYWORDS

cervical cancer, radiomics, lymph node metastasis, ultrasound, featurefusion, nomogram, deep transfer learning

# Introduction

Cervical cancer is a critical global health challenge, as it is the fourth most prevalent malignancy among women worldwide (1). The clinical management of this disease hinges on precise staging according to the International Federation of Gynecology and Obstetrics (FIGO) criteria, particularly the assessment of pelvic lymph node metastasis (PLNM), which fundamentally alters the therapeutic pathway (2, 3). Current National Comprehensive Cancer Network (NCCN) guidelines recommend radical hysterectomy with pelvic lymphadenectomy for stage IB-IIA lesions (4), yet emerging evidence questions this approach given that 70%-90% of patients with early-stage cervical cancer derive no oncological benefit from nodal dissection while facing substantial complication risks (2, 5). The 2018 revision of the FIGO criteria emphasized this prognostic stratification by introducing stage IIIC for radiologically suspected nodal involvement, and mandating chemoradiation over surgical intervention for these lesions (6). This staging evolution heightens the need for the accurate preoperative assessment of PLNM status, as treatment algorithms become increasingly dependent on imaging findings rather than surgical pathology (7). The reliable preoperative prediction of PLNM could significantly alter clinical management, potentially sparing node-positive patients from primary surgery and its associated morbidity, and instead directing them towards definitive chemoradiation, as supported by clinical evidence (8).

Unfortunately, current diagnostic modalities exhibit critical limitations in nodal evaluation, and the low incidence of intraoperatively confirmed nodal metastases (3.9%) despite

Abbreviations: DTL, deep transfer learning; PLNM, pelvic lymph node metastasis; AUC, area under the curve; DCA, decision curve analysis; FIGO, International Federation of Gynecology and Obstetrics; NCCN, National Comprehensive Cancer Network; ICC, intraclass correlation coefficients; CT, computed tomography; MRI, magnetic resonance imaging; PET, Positronemission tomography; BMI, body mass index; RBC, red blood cell; WBC, white blood cell; ALP, alkaline phosphatase; CEA, carcinoembryonic antigen; SCC, squamous cell carcinoma; LASSO, least absolute shrinkage and selection operator; ROI, region of interest; LR, logistic regression; SVM, support vector machines; KNN, k-nearest neighbors; MLP, multilayer perceptron.

preoperative imaging evaluation (9). Compared to CT, magnetic resonance imaging (MRI) demonstrates improved performance through functional sequences, yet a meta-analysis has revealed persistent interobserver variability exceeding 20% in lymph node characterization (10). Positron-emission tomography (PET)/CT, though valuable for metabolic assessment, suffers from limited accessibility and high false-negative rates in sub-centimeter nodes (11). Ultrasonography, the most widely available modality, shows operator-dependent accuracy, with its sensitivity differing according to the operator's experience (12). Sentinel lymph node biopsy is the most precise technique for assessing PLNM preoperatively; however, this approach is invasive, and its outcomes may be affected by factors such as atypical lymphatic drainage patterns, the effectiveness of preoperative lymphoscintigraphy, and the level of surgical expertise (13, 14). These diagnostic challenges have catalyzed innovation in quantitative imaging analysis.

Radiomics enables the high-throughput extraction of subvisual tumor features through the mathematical characterization of texture heterogeneity, margin irregularity, and vascular patterns (15), while deep learning (DL) techniques, especially convolutional neural network architectures, can identify intricate patterns and characteristics linked to lymph node metastasis (LNM). These advanced computational approaches significantly improve the precision of LNM prediction models (16). Although radiomic characteristics and DL-derived features each possess unique strengths and inherent constraints, the synergistic combination of these methodologies provides mutually reinforcing diagnostic insights. Consequently, this integrative approach has emerged as a significant focus area in contemporary medical imaging research (17). The multimodal fusion of handcrafted radiomic features and deep transfer learning (DTL)-derived biomarkers has improved diagnostic accuracy beyond single-modality approaches in breast cancers (18).

The biological rationale for the utility of ultrasonography in nodal assessment resides in its unique capacity to characterize dynamic tumor-stromal interactions through real-time functional imaging. Shear-wave elastography(SWE) provides biomechanical insights by measuring alterations in tissue stiffness caused by metastatic desmoplastic reactions, which are a critical discriminator between reactive and malignant lymph nodes (19).

This multifaceted capability for biological profiling positions ultrasonography as the ideal platform for developing predictive models that bridge radiological findings with underlying metastatic pathophysiology (20).

The clinical imperative for non-invasive nodal assessment extends beyond diagnostic accuracy. Unnecessary lymphadenectomy contributes to chronic lymphedema and increased healthcare costs (21, 22). In contrast, ultrasound-based predictive models offer cost-effective solutions adaptable to diverse healthcare settings. This methodology specifically addresses the limitations of prior MRI-centric radiomic models that require specialized sequences (such as diffusion-weighted imaging and apparent diffusion coefficient mapping), which are unavailable in low-resource regions. Currently, there is limited literature on the application of integrated models combining ultrasound radiomics and deep transfer learning for predicting pelvic lymph node metastasis in cervical cancer.

The primary objective of this investigation is to establish a clinically translatable decision-support tool that enables the noninvasive stratification of pelvic nodal metastasis risk in cervical cancer patients. Specifically, we aim to accomplish the following (1): validate ultrasound-derived radiomic signatures against surgical pathology in a 421-patient cohort (2); determine the complementary value of DTL-derived features in augmenting the value of the ultrasound-based radiomic signatures; and (3) develop an interpretable predictive model integrating quantitative imaging biomarkers with routine clinical and hematological parameters. This initiative directly responds to the guidelines of the European Society of Gynecological Oncology, European Society for Radiotherapy and Oncology, and European Society of Pathology, which advocate for precision-medicine approaches in gynecological oncology, while addressing healthcare disparities through ultrasound-centric technology, which is accessible across resource settings (23, 24).

# Methods

# Cohort selection

Patients from the First Affiliated Hospital of Guangxi Medical University undergoing radical hysterectomy with pelvic lymphadenectomy between May 2020 and September 2024 were screened against predefined eligibility criteria. Inclusion required the following (1): histopathologically confirmed cervical cancer with definitive PLNM status (2), preoperative transvaginal ultrasound imaging within 2 weeks before surgery capturing measurable lesions, and (3) availability of complete clinical records. Individuals meeting any of the following criteria were excluded from the study: prior oncological treatments (chemotherapy/radiotherapy), other concurrent gynecological malignancies, non-diagnostic ultrasound images, or incomplete data. From an initial pool of 963 candidates, 421 patients met the selection criteria and were enrolled in the study (Figure 1).

# Clinical and imaging data acquisition

We systematically extracted the following demographic, hematological, and histopathological parameters from the patients' electronic health records: age, parity, abortion history, body mass index (BMI), hematological indices (red blood cell [RBC] count, white blood cell [WBC] count, eosinophil count, and alkaline phosphatase [ALP]), levels of tumor markers (cancer antigen 125 [CA125], CA153, CA199, carcinoembryonic antigen [CEA], and squamous cell carcinoma [SCC] antigen), maximum lesion diameter, histological type, and PLNM status according to the postoperative pathological results (see the study design on Figure 2).

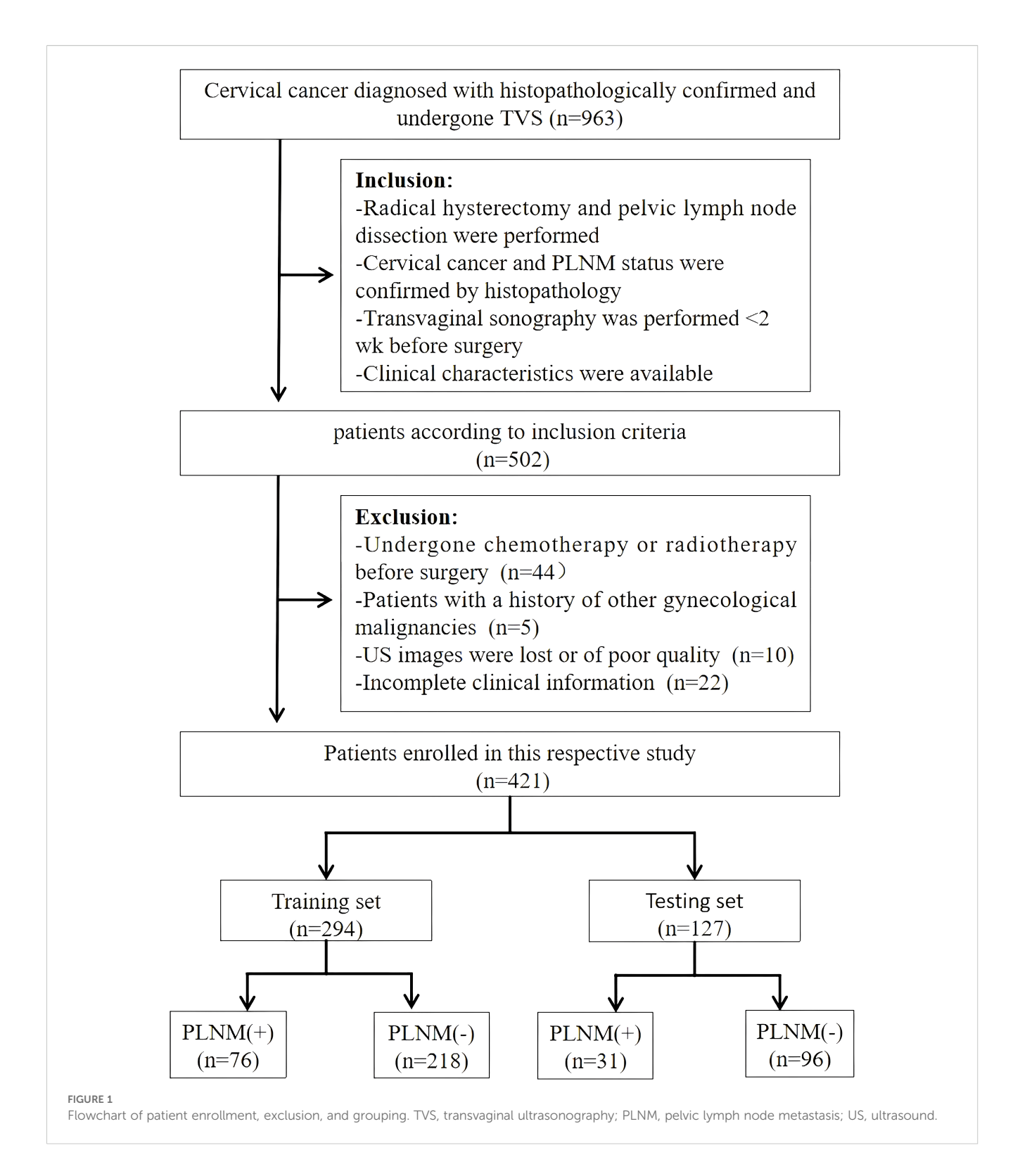
Ultrasound examinations were performed using the GE Voluson E10 and Logiq E9 systems equipped with 5–9 MHz transvaginal transducers. Standardized imaging protocols mandated bladder evacuation 10 min before the procedure, lithotomy positioning, and the acquisition of 6–10 representative images per patient in orthogonal planes. A single maximally cross-sectional image per patient was archived in the hospital's picture archiving system for blinded analysis by 2 sonographers with 5 and 11 years of experience. Discrepancies in lesion characterization were resolved through consensus review.

# Tumor segmentation and reproducibility assessment

Manual delineation of tumor boundaries was performed using ITK-SNAP ( $\nu 3.8.0$ ) on the selected ultrasound slices. To assess interobserver variability, we implemented a dual-annotation protocol: Sonographer A segmented all images, while Sonographer B independently annotated 50 randomly selected images. Intra-observer variability was assessed through repeated segmentations by Sonographer A after an 8-week interval. Features exhibiting intraclass correlation coefficients(ICCs) < 0.75 in both the interand intra-observer analyses were excluded to ensure robustness.

# Radiomic feature extraction and selection

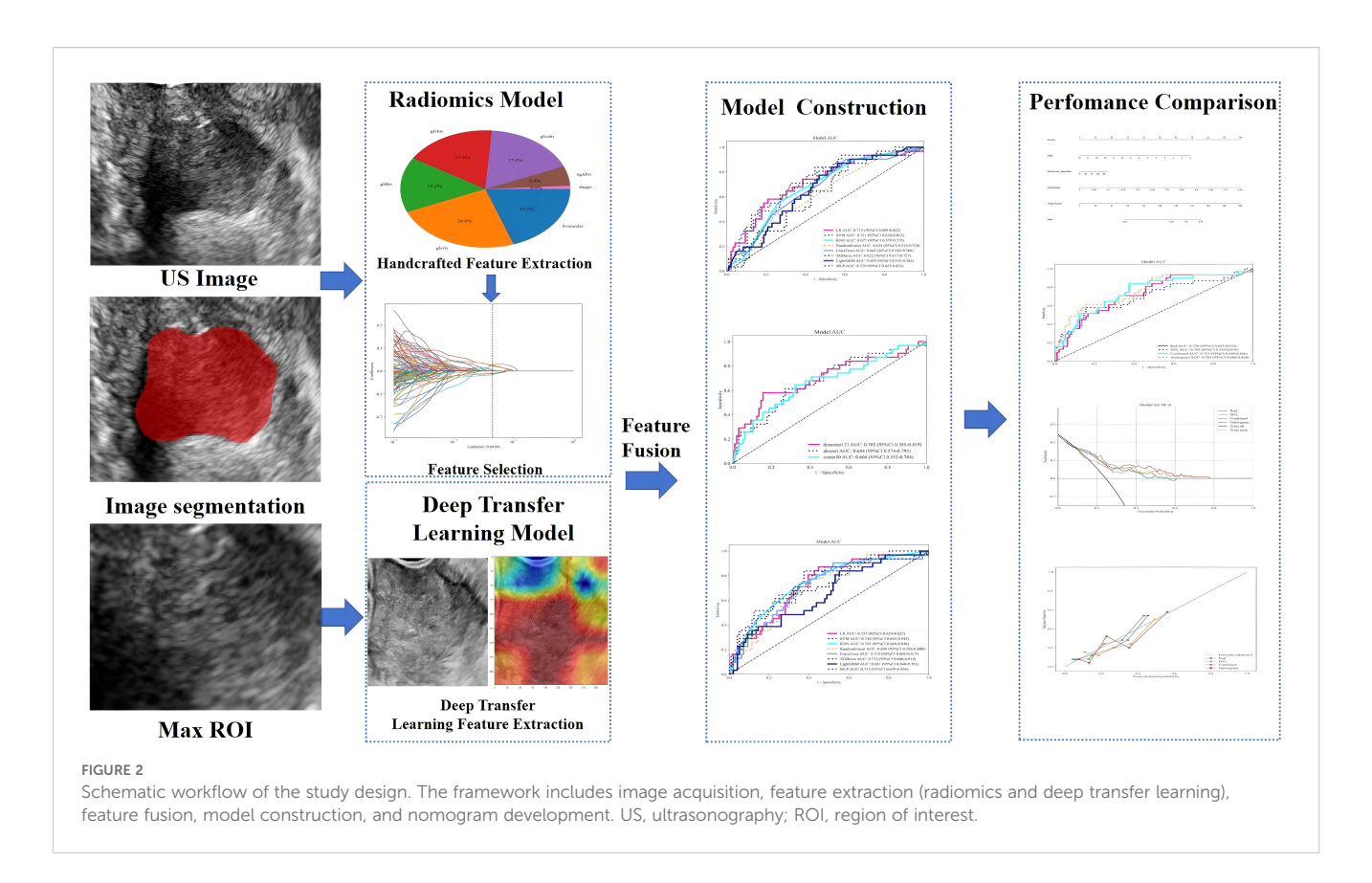
Quantitative radiomic profiling extracted 1,561 handcrafted features via PyRadiomics ( $\nu$ 3.0.1), categorized into the following 3 domains: geometric morphology (42 features), intensity distributions (744 features), and textural heterogeneity (775 features). Textural characterization employed 4 matrix-based methods: gray-level cooccurrence, gray-level run-length (GLRLM), gray-level size-zone, and neighboring gray tone difference matrices. A triphasic feature-reduction pipeline was applied (1): Mann-Whitney U tests (p < 0.05) identified metastasis-associated features (2); Spearman correlation filtering ( $|\rho| > 0.9$ ) eliminated redundant variables; and (3) least absolute shrinkage and selection operator (LASSO) regression with 10-fold cross-validation ( $\lambda$  = 0.0450, minimum criteria) selected 9 non-collinear predictors.



# Deep transfer learning architecture and optimization

Three convolutional neural networks DenseNet121, ResNet50, and AlexNet were adapted using transfer learning from ImageNet pretrained weights. Input images underwent region of interest

(ROI)-centered cropping to exclude extralesional tissue, followed by Z-score normalization. To enhance the generalizability of the images, we performed real-time data augmentation via random cropping ( $\pm$  15% volume), horizontal/vertical flipping (p = 0.5), and intensity scaling ( $\pm$  20%). Feature embeddings were extracted from the penultimate fully connected layer (16,383 dimensions)



of the optimal-performing network and reduced to 64 principal components via principal component analysis for computational efficiency.

balanced accuracy. The MLP architecture incorporated dropout

regularization (rate = 0.3) and early stopping (patience = 10

# Multimodal feature fusion strategy

Hybrid biomarkers were developed by concatenating the radiomic signatures with the DTL-derived principal components, thereby generating a 73-dimensional feature space. Recursive feature elimination was then performed, prioritizing variables that demonstrated complementary predictive value. After this step, 7 radiomic and 9 DTL components were retained. The fused feature set was standardized (using z-scores) prior to model integration.

# Predictive modeling framework

Eight machine learning classifiers were evaluated: logistic regression(LR; L2 regularization), support vector machines (SVM; radial basis kernel), k-nearest neighbors (KNN; k = 5), RandomForest (100 trees), ExtraTrees (50 trees), XGBoost (max\_depth = 6), LightGBM (num\_leaves = 31), and multilayer perceptron (MLP; 2 hidden layers, ReLU activation). Hyperparameter optimization employed a grid search with 10-fold cross-validation on the training cohort (70%, n = 294), prioritizing

# Clinical-radiomic nomogram development

Multivariate logistic regression identified independent clinical predictors (maximum tumor diameter and RBC count), which were integrated with the optimal fusion model outputs to construct a nomogram. Calibration slopes were adjusted using Platt scaling to align the predicted probabilities with the observed metastasis rates.

# Statistical validation protocol

epochs) to mitigate overfitting.

Model discrimination was quantified using area under the receiver operating characteristic curve (AUC). Calibration accuracy was assessed using the Hosmer-Lemeshow test and Brier scores. Decision curve analysis evaluated clinical utility across probability thresholds (0%–100%). Continuous variables were analyzed using the Mann-Whitney U test or Student t-test following Shapiro-Wilk normality testing, while categorical variables were evaluated using the chi-square or Fisher exact test. Correlation analyses were performed using Pearson (normal distribution) or Spearman (non-parametric) coefficients.

TABLE 1 Demographic and ultrasonographic characteristics of the study participants.

Feature	Training (N = 294)	PLNM (–)	PLNM (+)	P value	Testing (N = 127)	PLNM (–)	PLNM (+)	P value
Age	52.93 ± 10.68	52.78 ± 10.69	53.38 ± 10.72	0.671	51.98 ± 10.17	51.15 ± 10.22	54.55 ± 9.72	0.091
Parturition	2.46 ± 1.32	2.39 ± 1.28	2.64 ± 1.42	0.309	2.52 ± 1.48	2.40 ± 1.51	2.90 ± 1.35	0.037
Abortion	1.41 ± 1.38	1.41 ± 1.39	1.43 ± 1.38	0.767	1.30 ± 1.32	1.34 ± 1.40	1.16 ± 1.07	0.726
BMI	23.35 ± 3.53	23.29 ± 3.43	23.52 ± 3.82	0.596	23.29 ± 3.39	23.47 ± 3.54	22.75 ± 2.83	0.594
RBC count (10 <sup>12</sup> /L)	4.09 ± 0.91	4.12 ± 0.99	3.99 ± 0.59	0.500	4.05 ± 0.62	4.09 ± 0.56	3.90 ± 0.78	0.138
WBC count (10 <sup>^9</sup> /L)	11.14 ± 3.62	11.31 ± 3.65	10.64 ± 3.52	0.163	11.26 ± 3.86	11.66 ± 3.98	10.01 ± 3.22	0.027
ALP (U/L)	63.08 ± 19.26	61.86 ± 19.22	66.59 ± 19.06	0.015	65.13 ± 22.48	61.36 ± 18.33	76.81 ± 29.53	0.003
Eosinophil count (10^9/L)	0.16 ± 1.23	0.18 ± 1.42	0.10 ± 0.22	<0.001	0.05 ± 0.10	0.04 ± 0.10	0.06 ± 0.09	0.122
CA125 (U/mL)	37.53 ± 117.05	26.16 ± 49.86	70.13 ± 211.85	<0.001	34.93 ± 73.63	25.58 ± 61.65	63.91 ± 97.91	<0.001
CA153 (U/mL)	14.31 ± 8.95	13.66 ± 9.03	16.15 ± 8.48	0.008	13.27 ± 7.33	12.69 ± 6.80	15.04 ± 8.67	0.21
CA199 (U/mL)	46.76 ± 390.57	13.23 ± 24.10	142.92 ± 762.65	<0.001	21.87 ± 86.47	25.11 ± 99.00	11.82 ± 15.04	0.31
CEA (U/mL)	6.04 ± 16.58	5.08 ± 10.85	8.80 ± 26.89	0.024	4.14 ± 6.14	3.43 ± 5.10	6.34 ± 8.33	0.002
SCC antigen (ng/mL)	6.17 ± 9.99	5.00 ± 8.47	9.53 ± 12.92	0.002	6.91 ± 12.64	3.87 ± 5.90	16.32 ± 20.96	<0.001
Maximum diameter (mm)	33.10 ± 13.55	30.25 ± 11.86	41.29 ± 14.81	<0.001	31.83 ± 11.84	29.47 ± 10.91	39.16 ± 11.77	<0.001
Histology				0.167				0.075
Squamous cell carcinoma	231 (78.57)	174 (79.82)	57 (75.00)		101 (79.53)	72 (75.00)	29 (93.55)	
Adenocarcinoma	48 (16.33)	36 (16.51)	12 (15.79)		19 (14.96)	18 (18.75)	1 (3.23)	
Others	15 (5.10)	8 (3.67)	7 (9.21)		7 (5.51)	6 (6.25)	1 (3.23)	

PLNM, pelvic lymph node metastasis; BMI, body mass index; RBC, red blood cell; WBC, white blood cell; ALP, alkaline phosphatase; CA, cancer antigen; CEA, carcinoembryonic antigen; SCC antigen, squamous cell carcinoma antigen.

# Computational infrastructure

All analyses were implemented using Python v3.9 (scikit-learn v1.2, PyTorch v1.13) on an NVIDIA A100 GPU cluster. Reproducibility was ensured through fixed random seeds (NumPy = 42, PyTorch = 3407) and version-controlled pipelines.

# Results

# Clinical and ultrasound characteristics

This retrospective analysis included 421 cervical cancer patients, of whom 294 patients were allocated to the training cohort (218 [74.1%] PLNM-negative patients; 76 [25.9%] PLNM-positive patients) and 127 to the testing cohort (96 [75.6%] PLNM-negative patients; 31 [24.4%] PLNM-positive patients; Table 1). The PLNM-negative and PLNM-positive groups significantly differed in terms of parturition (p=0.037), WBC count (p=0.027), ALP level (p=0.003), CA125 level (p<0.001), CEA level (p=0.002), SCC antigen level (p<0.001), and maximum tumor diameter (p<0.001). No significant differences were detected in age, abortion history, BMI, RBC count, and histology. Cohort stratification ensured balanced clinical characteristics between the training and testing sets (p>0.05 for all variables).

Univariate logistic regression identified age, parturition, abortion, BMI, RBC count, WBC count, ALP level, CA153 level, histology, and maximum tumor diameter as potential predictors of PLNM status (Table 2). Subsequent multivariate analysis confirmed maximum tumor diameter (odds ratio [OR] = 1.055, 95% confidence interval [CI]: 1.036–1.075) and RBC count (OR = 0.646, 95% CI: 0.459–0.910) as independent risk factors for PLNM.

# Radiomics model development

A total of 1,561 handcrafted radiomic features were extracted from the ultrasound images, and distributed across the geometric (n = 42), intensity-based (n = 744), and texture-based (n = 775) categories (Figure 3). Feature selection involved redundancy elimination via Spearman correlation ( $|\rho| > 0.8$ ) followed by LASSO regression ( $\lambda$  = 0.0450, 10-fold cross-validation), and yielded 9 robust handcrafted radiomic features (Figures 4, 5). The importance scores of these features, ranked by absolute LASSO coefficients, are visualized in Figure 4B.

Eight machine-learning classifiers were evaluated using the selected handcrafted radiomic features (Table 3). The MLP model demonstrated optimal performance in the testing cohort (AUC = 0.729, 95% CI: 0.6249-0.8334), outperforming the logistic

TABLE 2 Univariate and multivariate logistic regression analysis of clinical predictors for PLNM.

	Univariate	e analysis			Multivaria	te analysis		
Clinical and US characteristics	OR	Lower 95% CI	Upper 95% CI	P	OR	Lower 95% CI	Upper 95% CI	Р
Age	0.981	0.977	0.985	0.000	0.994	0.971	1.017	0.667
Parturition	0.730	0.672	0.792	0.000	1.155	0.951	1.404	0.222
Abortion	0.667	0.591	0.745	0.000	1.085	0.909	1.294	0.446
BMI	0.957	0.948	0.966	0.000	0.936	0.881	0.995	0.073
RBC count	0.771	0.731	0.815	0.000	0.646	0.459	0.910	0.036
WBC count	0.911	0.894	0.930	0.000	0.965	0.904	1.031	0.379
ALP	0.986	0.982	0.989	0.000	1.006	0.993	1.020	0.460
Eosinophil count	0.628	0.211	1.865	0.482				
CA125	1.000	0.998	1.001	0.860				
CA153	0.952	0.939	0.966	0.000	1.010	0.985	1.036	0.507
CA199	1.001	1.000	1.002	0.363				
CEA	0.988	0.974	1.003	0.182				
SCC antigen	0.981	0.964	0.999	0.077				
Maximum tumor diameter	0.981	0.974	0.986	0.000	1.055	1.036	1.075	0.000
Histology	0.602	0.427	0.848	0.015	1.410	0.911	2.181	0.196

PLNM, pelvic lymph node metastasis; US, ultrasonography; OR, odds ratio; CI, confidence interval; BMI, body mass index; RBC, red blood cell; WBC, white blood cell; ALP, alkaline phosphatase; CA, cancer antigen; CEA, carcinoembryonic antigen; SCC antigen, squamous cell carcinoma antigen.

regression (AUC = 0.715), support vector machine (AUC = 0.711), and other classifiers (Figure 6).

# Deep transfer learning model performance

Three pre-trained convolutional neural networks (DenseNet121, ResNet50, and AlexNet) were adapted for DTL analysis (Table 4). DenseNet121 achieved the highest testing AUC of 0.702 (95% CI: 0.5853–0.8193), surpassing ResNet50 (AUC = 0.668) and AlexNet (AUC = 0.684; Figure 7). Gradient-weighted Class Activation Mapping was used to localize the tumor subregions that were critical for the predictions made by DenseNet121, and the results revealed preferential attention to areas of heterogeneous echogenicity (Figure 8).

### Feature fusion and combined model

After recursive feature elimination, a total of 7 handcrafted radiomic features and 9 DTL features were retained from the fused feature set comprising 1625 dimensions (Figures 9, 10). Among the 8 classifiers evaluated (Table 5), the MLP-based fusion model achieved a testing AUC of 0.753 (95% CI: 0.6494–0.8560), representing a 5.1% improvement over standalone DenseNet121 (AUC: 0.753 vs.0.702; Figure 11).

# Nomogram construction and validation

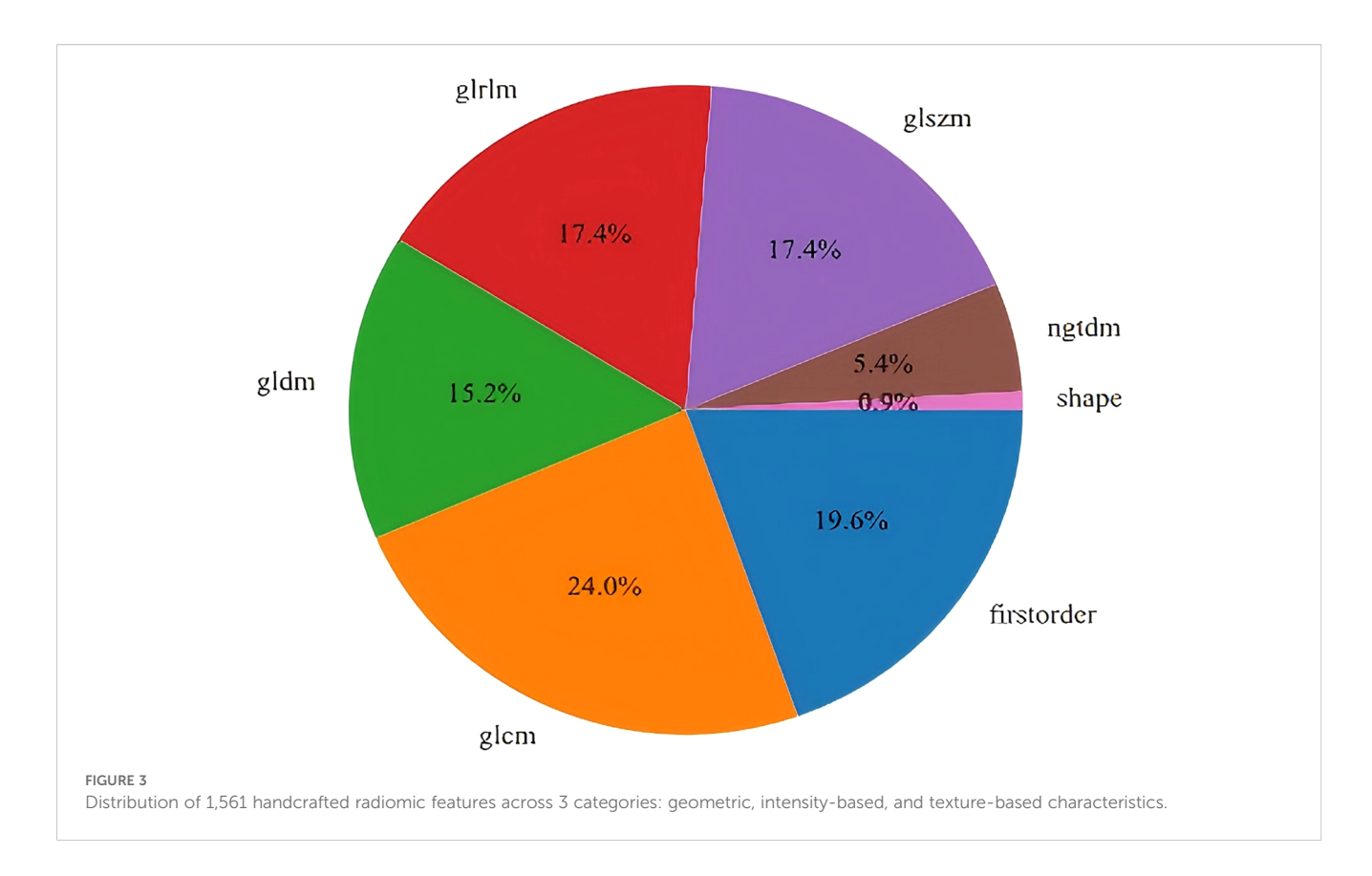
The fusion model was combined with independent clinical predictors (maximum tumor diameter and RBC count) to develop a nomogram (Figure 12). The nomogram exhibited superior discrimination, with training and testing AUCs of 0.871 (95% CI: 0.8274–0.9156) and 0.764 (95% CI: 0.6604–0.8678), respectively, outperforming the radiomics, DTL, and fusion models (Table 6, Figure 13). Calibration curves demonstrated excellent agreement between the predicted and observed PLNM probabilities in both cohorts (Hosmer-Lemeshow test: training, p = 0.072; testing, p = 0.131; Figure 14). Decision curve analysis confirmed that the nomogram provided a greater net benefit across clinically relevant threshold probabilities (10%–50%) than that associated with alternative models (Figure 15).

# Discussion

# Radiomics and deep learning synergy

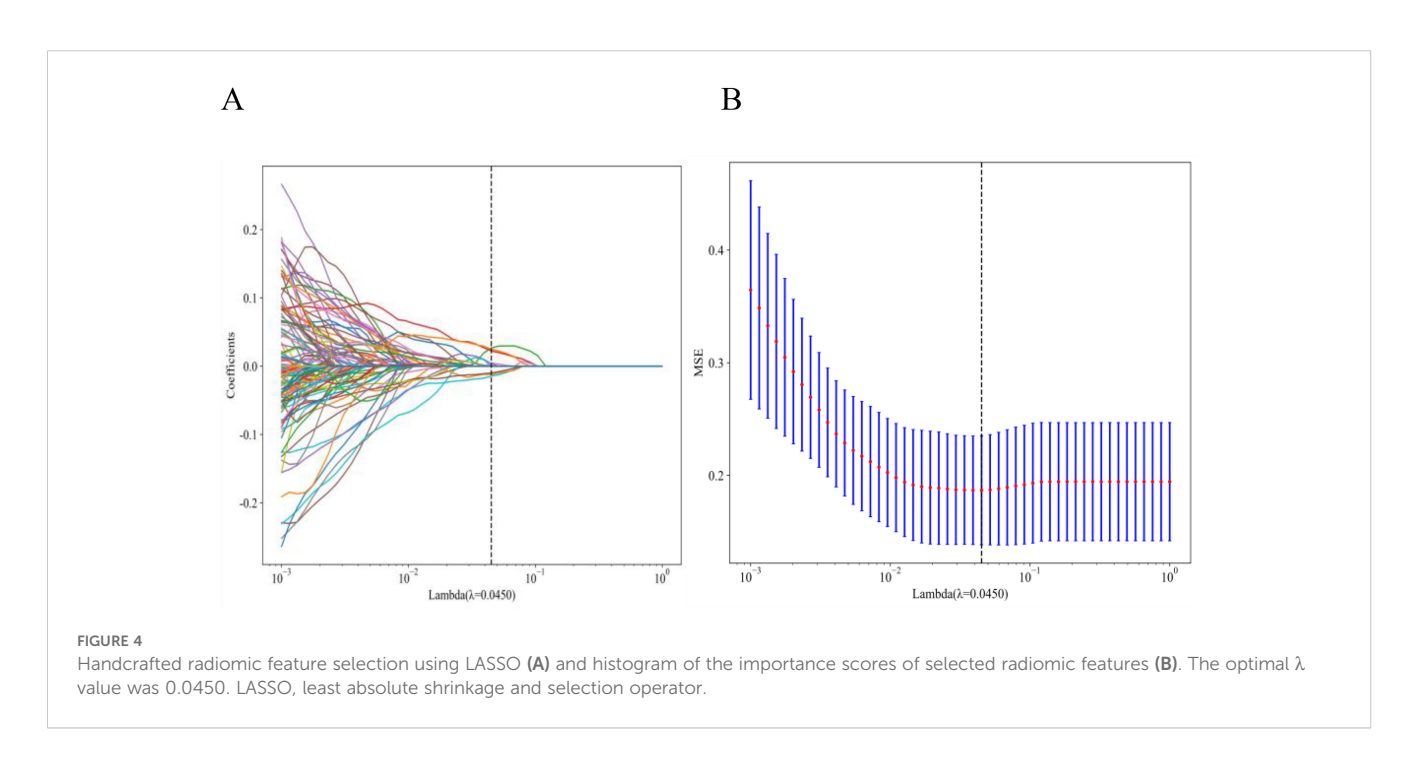
While the acquisition of ultrasound images may be subject to operator variability,

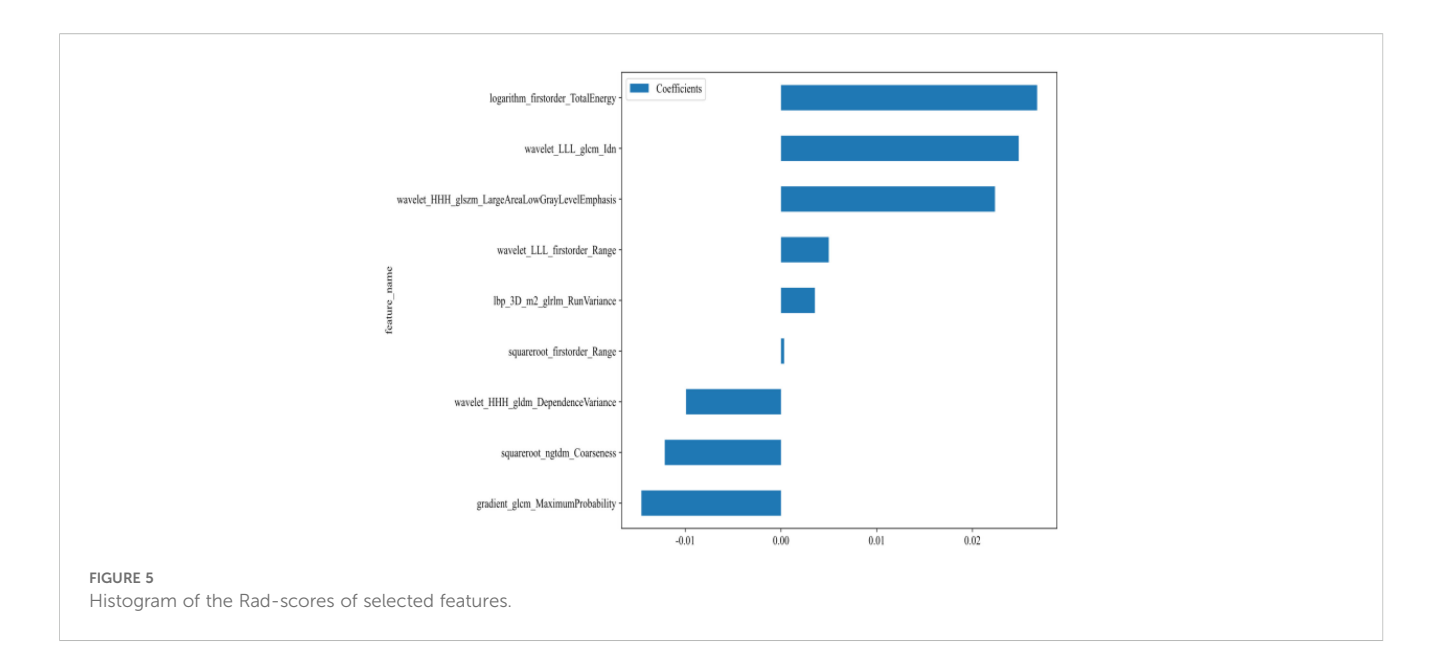
quantitative characterization of tumor heterogeneity through radiomic feature extraction enables the objective assessment of metastatic propensity, thereby circumventing subjective variability



in image interpretation (25). In our study, we implemented several strategies to enhance robustness against operator variability. First, all sonographers followed a standardized imaging protocol to minimize acquisition differences. More importantly, during feature extraction, we performed a rigorous reproducibility assessment based on both inter- and intra-observer intraclass correlation coefficients (ICCs). Features with ICCs below 0.75

were excluded, ensuring that only stable and reproducible features were used for model construction. This process helps to filter out features that are highly sensitive to segmentation differences or acquisition parameters, thereby increasing the generalizability and reliability of the radiomic signature (26, 27). Future studies employing automated segmentation algorithms could further reduce this potential source of variability. Earlier research has





demonstrated that radiomics-based approaches can effectively predict lymph node metastasis across various cancer types (25, 28, 29). The radiomic component of our model demonstrated robust validation performance (testing AUC = 0.729), which was consistent with the performance of MRI-based radiomic prediction of nodal involvement (AUC = 0.83) in a meta-analysis

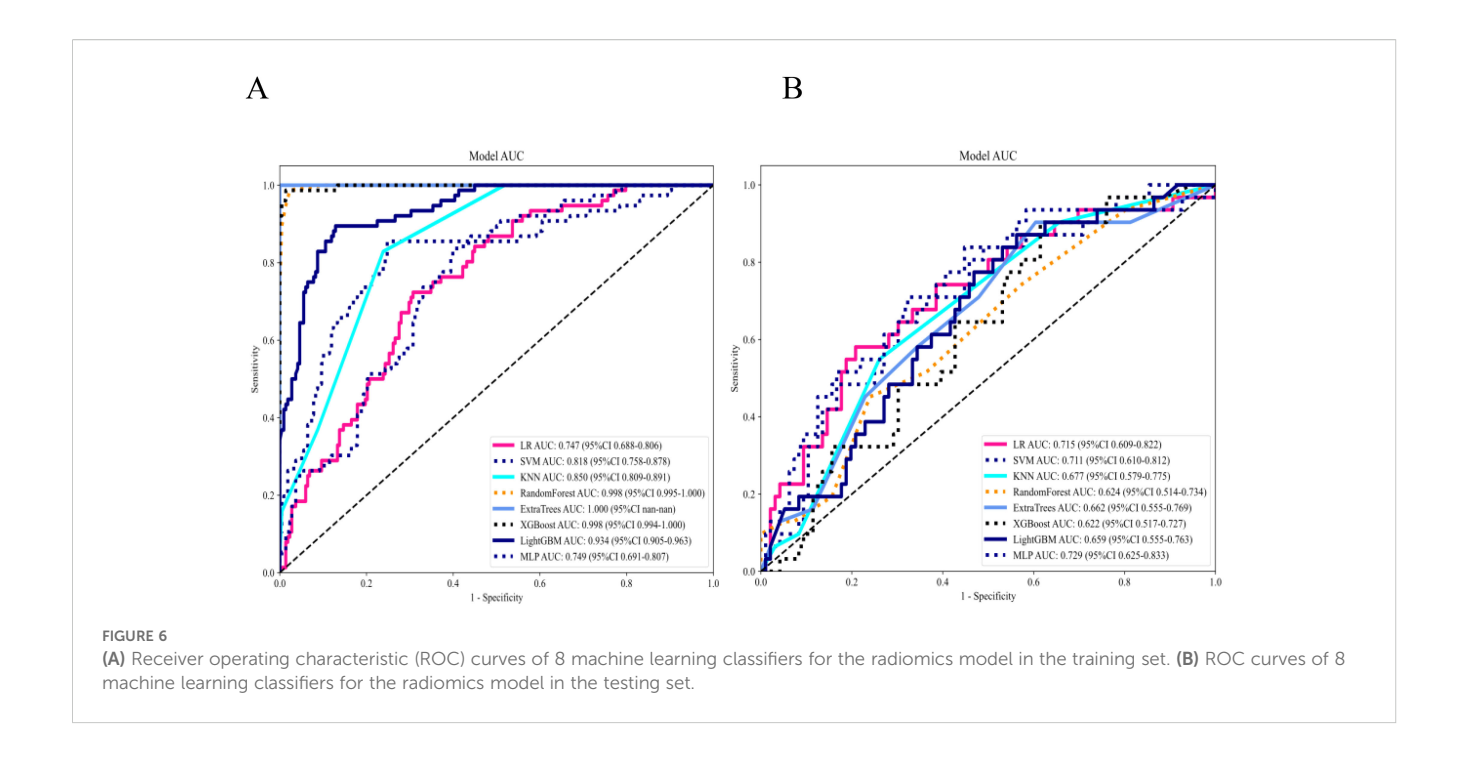
of cervical cancer patients (9). This concordance suggests the potential of ultrasound-based radiomics as a cost-effective alternative to advanced imaging modalities, particularly in resource-constrained settings.

DL, a subset of machine learning, enables computational models featuring multiple processing layers to acquire hierarchical

TABLE 3 Diagnostic performance of radiomic models using different classifiers.

Model	AUC	95% CI	Accuracy	Sensitivity	Specificity	PPV	NPV
LR-Training	0.747	0.6877-0.8059	0.697	0.711	0.693	0.446	0.873
SVM-Training	0.818	0.7583-0.8781	0.776	0.842	0.752	0.542	0.932
KNN-Training	0.850	0.8093-0.8914	0.772	0.368	0.913	0.596	0.806
RandomForest-Training	0.998	0.9950-1.0000	0.976	0.947	0.986	0.960	0.982
ExtraTrees-Training	1.000	1.0000-1.0000	0.741	0.000	1.000	0.000	0.741
XGBoost-Training	0.998	0.9941-1.0000	0.983	0.974	0.986	0.961	0.991
LightGBM-Training	0.934	0.9051-0.9633	0.874	0.882	0.872	0.705	0.955
MLP-Training	0.749	0.6906-0.8071	0.653	0.829	0.592	0.414	0.908
LR-Testing	0.715	0.6086-0.8222	0.732	0.548	0.792	0.459	0.844
SVM-Testing	0.711	0.6095-0.8118	0.614	0.806	0.552	0.368	0.898
KNN-Testing	0.677	0.5785-0.7750	0.717	0.097	0.917	0.273	0.759
RandomForest-Testing	0.624	0.5141-0.7342	0.685	0.194	0.844	0.286	0.764
ExtraTrees-Testing	0.662	0.5553-0.7693	0.567	0.710	0.521	0.324	0.847
XGBoost-Testing	0.622	0.5167-0.7266	0.504	0.871	0.385	0.314	0.902
LightGBM-Testing	0.659	0.5554-0.7632	0.535	0.839	0.437	0.325	0.894
MLP-Testing	0.729	0.6249-0.8334	0.677	0.677	0.677	0.404	0.867

AUC, area under the curve; CI, confidence interval; PPV, positive predictive value; NPV, negative predictive value; LR, logistic regression; SVM, support vector machine; KNN, k-nearest neighbor; XGBoost, eXtreme gradient boost; LightGBM, light gradient boosting machine; MLP, multilayer perceptron.



representations of data across various levels of abstraction (30). In numerous real-world scenarios, convolutional neural networks that have been initially trained on the ImageNet dataset are widely utilized, a technique commonly referred to as transfer learning (31, 32). In our study, DTL architectures exhibited paradoxical performance characteristics, with superior training accuracy (AUC = 0.782) versus diminished validation metrics (AUC = 0.702). This performance gap aligns with findings in gastrointestinal oncology research, where DTL models consistently exhibit a higher risk of overfitting than radiomic approaches (33, 34). In our study, the DTL model was inferior to the conventional radiomic model in the testing set. The possible reasons for this are as follows: First, DTL requires a large number of training sets, whereas this is a single-center study; a large multi-center is needed for further training in the future. Second, despite the strong performance of DTL in diverse classification and prediction tasks, its inherent lack of interpretability, characteristic of black-box algorithms, limits its

broader applicability (35, 36). Future iterations incorporating three-dimensional ROI reconstructions and attention mechanisms may enhance the generalizability of DTL (37).

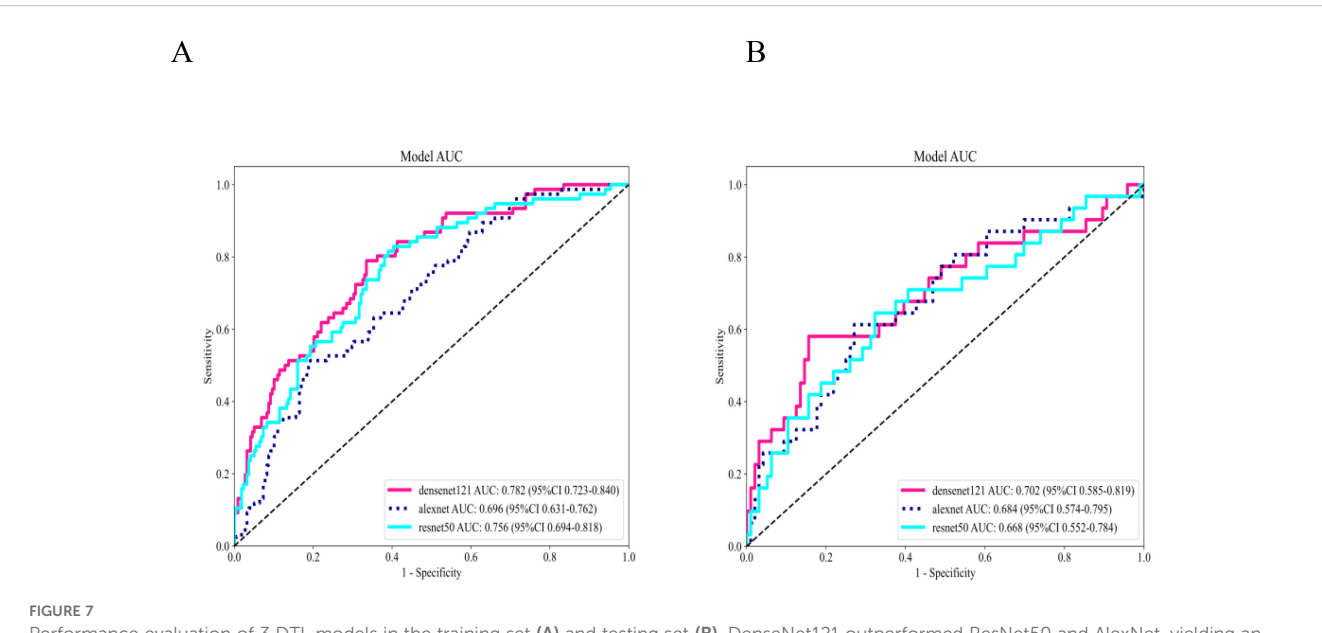
# Advantages of multimodal fusion

The feature-level integration of radiomic and DTL biomarkers generated synergistic diagnostic improvements, with the testing AUC (0.753) of the fusion model exceeding those of standalone approaches. This aligns with the findings of Wang et al., who found that the fusion of radiomics and deep learning features achieved a testing AUC of 0.934 for differentiating benign and malignant parotid gland tumors, significantly surpassing standalone radiomics (AUC = 0.853) and deep learning models (AUC = 0.883) (16). The fusion model demonstrated enhanced capability in detecting small metastatic foci (<5 mm) by leveraging complementary features: radiomics quantified

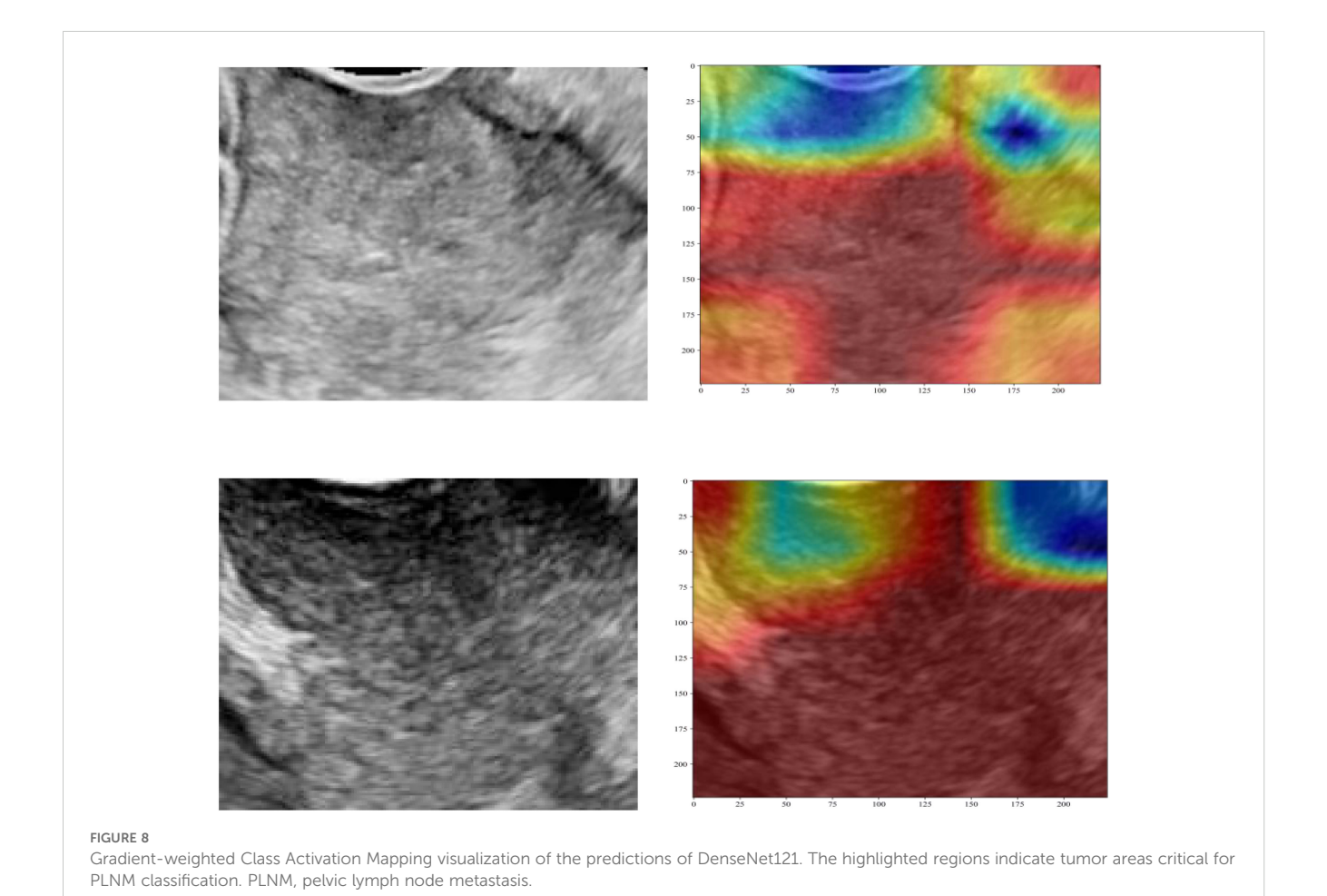
TABLE 4 Comparison of deep transfer learning models for PLNM prediction.

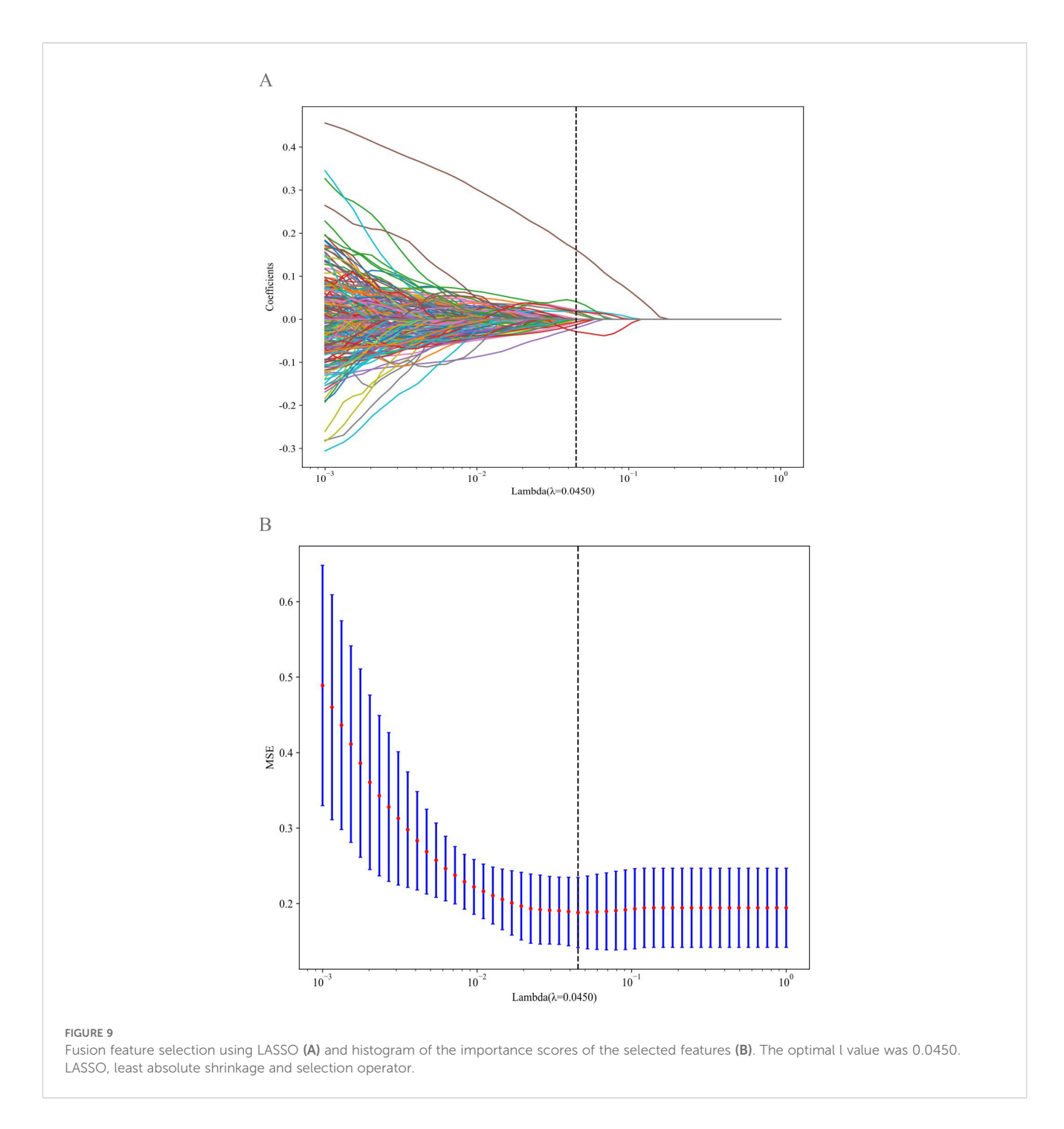
Model	AUC	95% CI	Accuracy	Sensitivity	Specificity	PPV	NPV
DenseNet121-Training	0.782	0.7231-0.8400	0.694	0.776	0.665	0.447	0.895
AlexNet-Training	0.696	0.6306-0.7622	0.728	0.500	0.807	0.475	0.822
ResNet50-Training	0.756	0.6939-0.8179	0.660	0.803	0.610	0.418	0.899
DenseNet121-Testing	0.702	0.5853-0.8193	0.772	0.548	0.844	0.531	0.853
AlexNet-Testing	0.684	0.5742-0.7947	0.693	0.581	0.729	0.409	0.843
ResNet50-Testing	0.668	0.5516-0.7837	0.661	0.613	0.677	0.380	0.844

PLNM, pelvic lymph node metastasis; AUC, area under the curve; CI, confidence interval; PPV, positive predictive value; NPV, negative predictive value.



Performance evaluation of 3 DTL models in the training set (A) and testing set (B). DenseNet121 outperformed ResNet50 and AlexNet, yielding an AUC of 0.702 in the testing set. DTL, deep transfer learning; AUC, area under the curve.

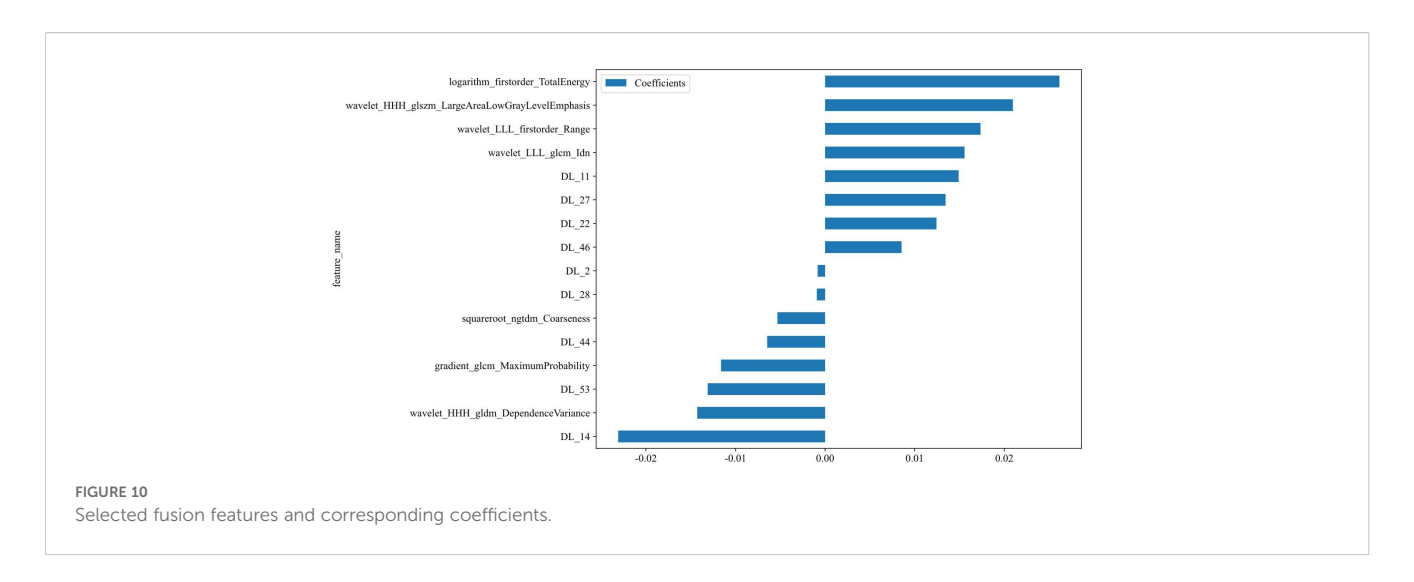




margin irregularities (e.g., GLRLM\_ShortRunEmphasis), while DTL identified subtle perilesional vascular patterns. This multimodal synergy directly addresses the longstanding limitation of conventional imaging in identifying micrometastases—a challenge highlighted in studies such as that by Liu et al. (2017), who found that conventional CT criteria (e.g., size thresholds) struggled to detect subcentimeter nodal metastases in esophageal cancer (38). By integrating heterogeneous biomarkers, the fusion approach overcomes the sensitivity-precision trade-off inherent to single-modality methods, aligning with advancements in radiomics-deep learning fusion frameworks observed in other oncologic contexts (17, 38).

# Toward a multiparametric ultrasound fusion model

Our study utilized conventional B-mode ultrasound images, which are the most widely available and cost-effective. However, we acknowledge that emerging ultrasound technologies such as three-dimensional (3D) ultrasonography can provide additional quantitative information on tumor volume. Volumetric data from 3D imaging captures the full spatial complexity of a tumor (39). SWE offers unique insights into underlying biological characteristics. Tissue stiffness, as measured by SWE, often



correlates with pathological processes such as fibrosis and cellular proliferation, which are hallmarks of malignancy (19, 40, 41). Contrast-enhanced ultrasonography can assess the vitality of tumors through contrast enhancement, and can depict the real-time dynamic perfusion of tumors (42). These parameters have shown promise in characterizing tumor aggressiveness and predicting lymph node metastasis. Integrating these multiparametric ultrasound features into our fusion model represents a compelling direction for future research, potentially further boosting predictive accuracy.

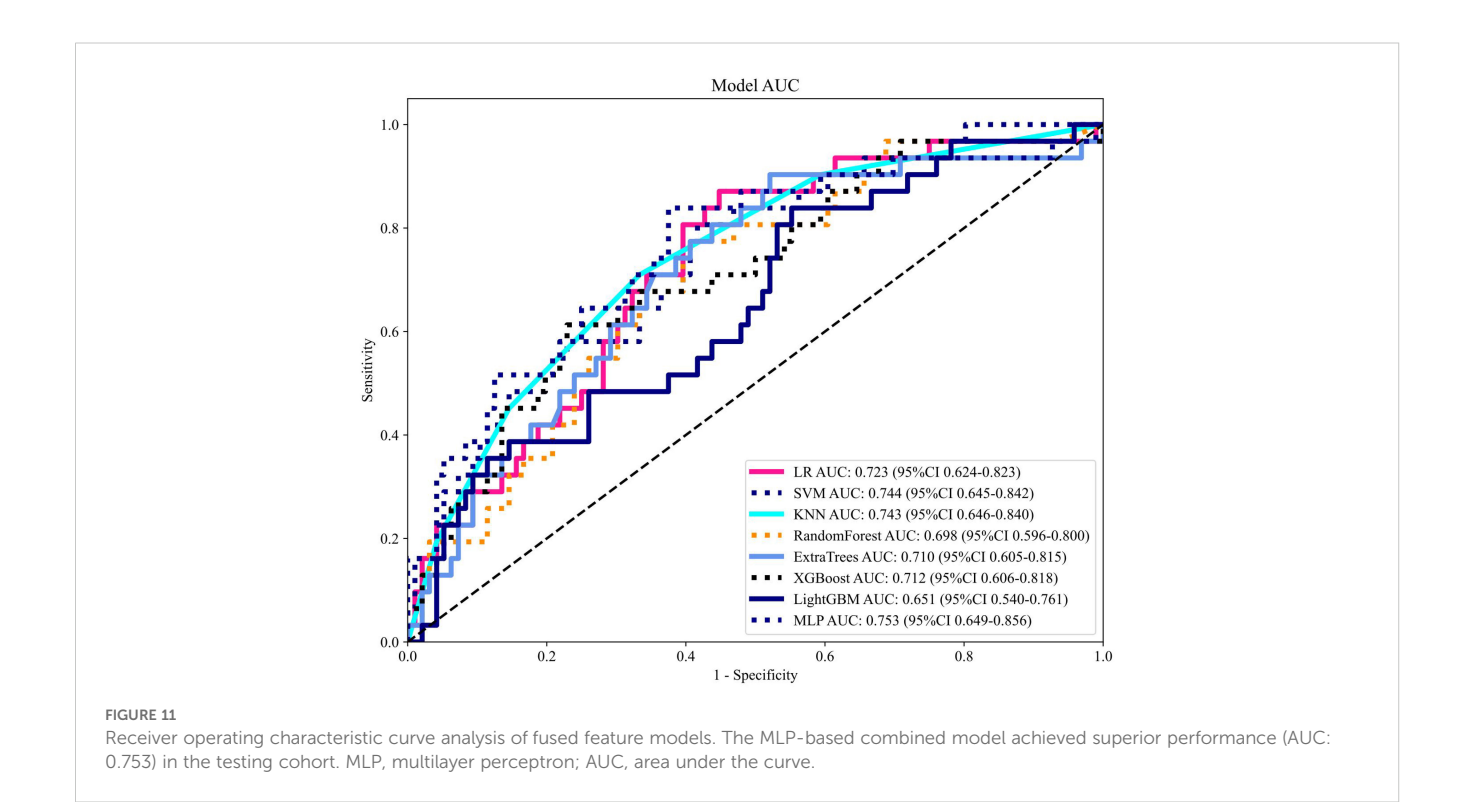
# Clinical parameter integration

Multivariate analysis identified maximum tumor diameter (OR = 1.055) and RBC count (OR = 0.646) as independent predictors of PLNM, corroborating established oncopathological mechanisms. Numerous research studies have indicated that tumor size serves as a standalone predictor for lymph node metastasis in cervical cancer; tumor size directly correlates with the probability of lymphatic invasion (43, 44). Thus, large tumors (tumor diameter > 4 cm) are a risk factor for nodal metastasis and considerably

TABLE 5 Performance evaluation of feature fusion models across classifiers.

Model	AUC	95% CI	Accuracy	Sensitivity	Specificity	PPV	NPV
LR-Training	0.831	0.7768-0.8858	0.820	0.658	0.876	0.649	0.880
SVM-Training	0.922	0.8810-0.9627	0.857	0.921	0.835	0.660	0.968
KNN-Training	0.861	0.8179-0.9031	0.820	0.513	0.927	0.709	0.845
RandomForest-Training	0.869	0.8204-0.9176	0.776	0.816	0.761	0.544	0.922
ExtraTrees-Training	0.828	0.7727-0.8833	0.728	0.816	0.697	0.484	0.916
XGBoost-Training	0.975	0.9580-0.9924	0.935	0.895	0.950	0.861	0.963
LightGBM-Training	0.937	0.9051-0.9693	0.878	0.882	0.876	0.713	0.955
MLP-Training	0.857	0.8086-0.9064	0.762	0.829	0.739	0.525	0.925
LR-Testing	0.723	0.6243-0.8226	0.622	0.839	0.552	0.377	0.914
SVM-Testing	0.744	0.6451-0.8422	0.630	0.774	0.583	0.375	0.889
KNN-Testing	0.743	0.6451-0.8422	0.756	0.452	0.854	0.500	0.828
RandomForest-Testing	0.698	0.5956-0.8003	0.630	0.742	0.594	0.371	0.877
ExtraTrees-Testing	0.710	0.6053-0.8154	0.575	0.871	0.479	0.351	0.920
XGBoost-Testing	0.712	0.6058-0.8176	0.724	0.581	0.771	0.450	0.851
LightGBM-Testing	0.651	0.5399-0.7612	0.535	0.806	0.448	0.321	0.878
MLP-Testing	0.753	0.6494-0.8560	0.669	0.806	0.625	0.410	0.909

AUC, area under the curve; CI, confidence interval; PPV, positive predictive value; NPV, negative predictive value; LR, logistic regression; SVM, support vector machine; KNN, k-nearest neighbor; XGBoost, eXtreme gradient boost; LightGBM, light gradient boosting machine; MLP, multilayer perceptron.



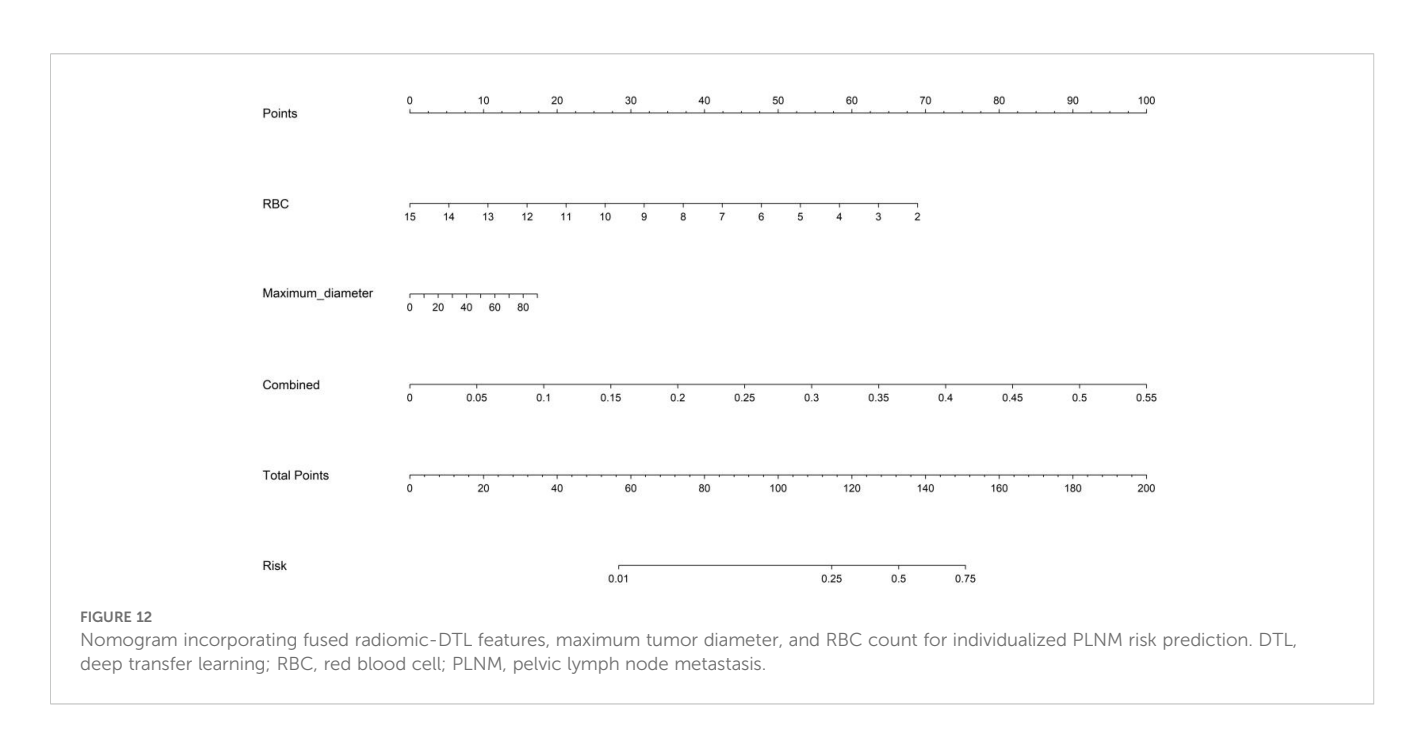


TABLE 6 Comparison of AUCs of radiomics, DTL, fusion, and nomogram models.

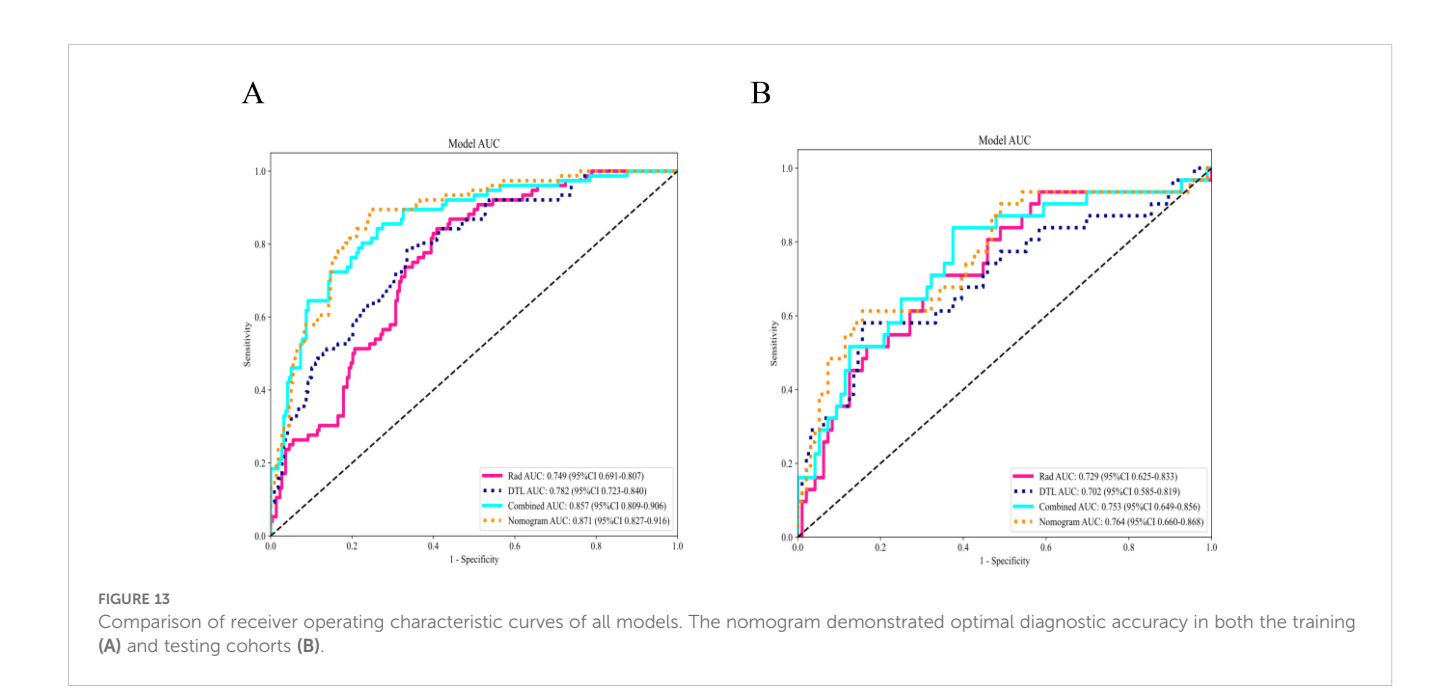
Model	AUC	95% CI	Accuracy	Sensitivity	Specificity	PPV	NPV
Radiomics-Training	0.749	0.6906-0.8071	0.653	0.829	0.592	0.414	0.908
DTL-Training	0.782	0.7231-0.8400	0.694	0.776	0.665	0.447	0.895
Fusion-Training	0.857	0.8086-0.9064	0.762	0.829	0.739	0.525	0.925

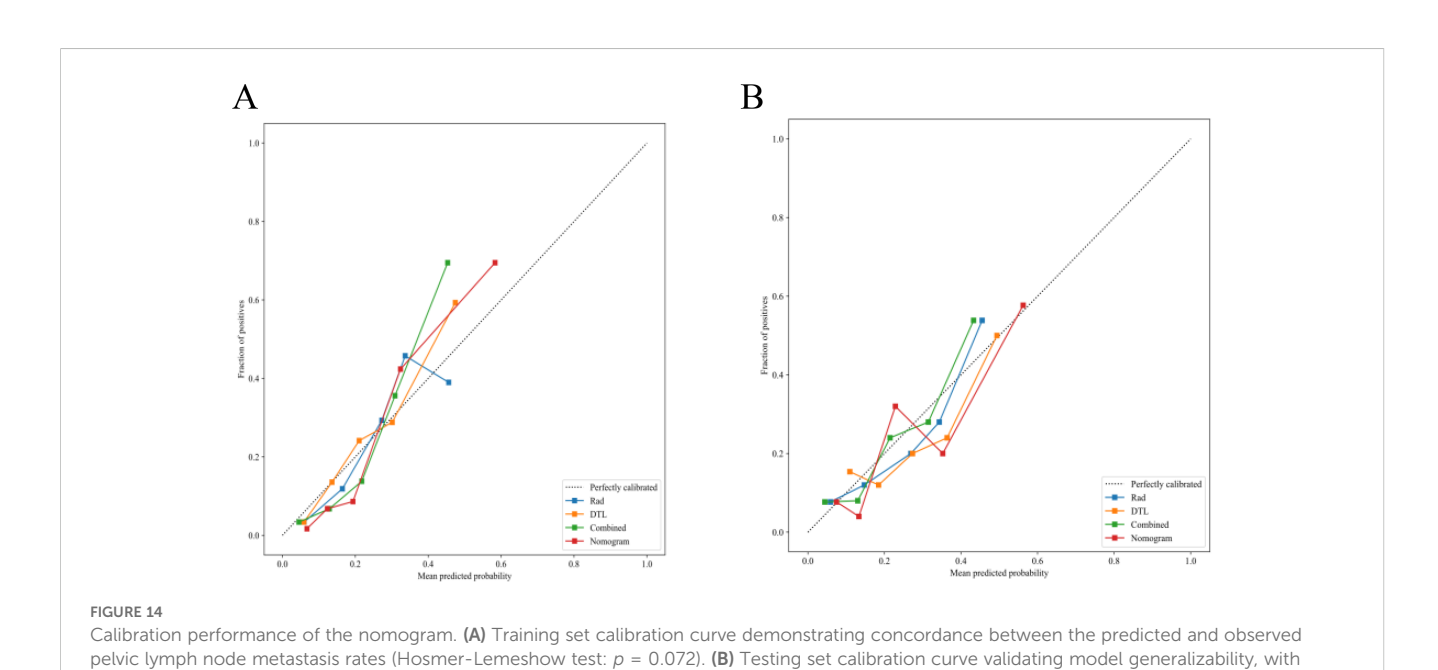
(Continued)

TABLE 6 Continued

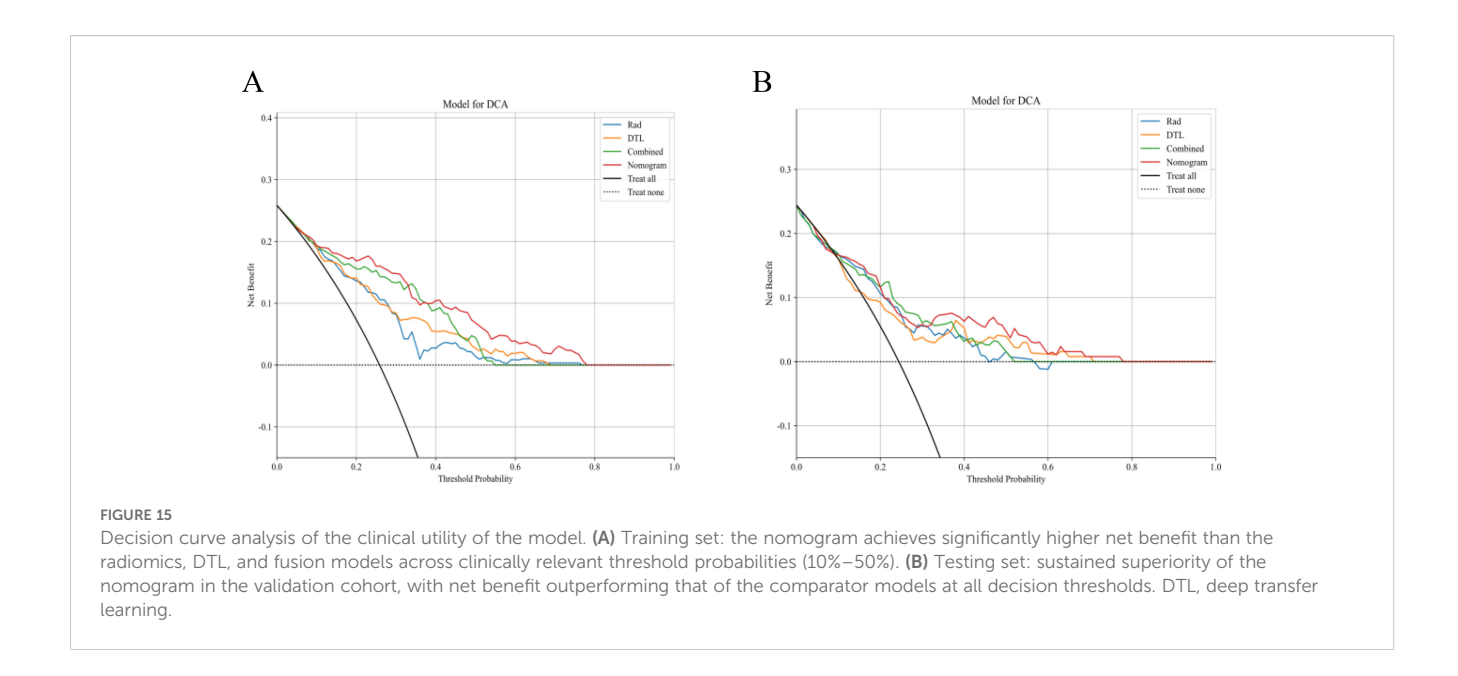
Model	AUC	95% CI	Accuracy	Sensitivity	Specificity	PPV	NPV
Nomogram-Training	0.871	0.8274-0.9156	0.789	0.882	0.757	0.558	0.948
Radiomics-Testing	0.729	0.6249-0.8334	0.677	0.677	0.677	0.404	0.867
DTL-Testing	0.702	0.5853-0.8193	0.772	0.548	0.844	0.531	0.853
Fusion-Testing	0.753	0.6494-0.8560	0.669	0.806	0.625	0.410	0.909
Nomogram-Testing	0.764	0.6604-0.8678	0.780	0.581	0.844	0.545	0.862

AUC, area under the curve; DTL, deep transfer learning; CI, confidence interval; PPV, positive predictive value; NPV, negative predictive value; Fusion, radiomics-DTL fusion model.





maintained agreement between predictions and outcomes (Hosmer-Lemeshow test: p = 0.131).



increase the incidence of PLNM (45). Conversely, anemia (reflected by a low RBC count) can be associated with chronic tumor hemorrhage and inflammatory microenvironment modifications that are conducive to metastatic spread (46). Considering the influence of clinical factors on PLNM, we developed a nomogram incorporating the radiomics signature, the DTL signature, maximum tumor diameter, and RBC count. The nomogram displayed good calibration and excellent performance to evaluate PLNM status with an AUC of 0.871 in the training cohort and 0.764 in the test cohort. The incorporation of these clinical parameters with imaging biomarkers in the nomogram created a biologically plausible decision tool that outperformed single-modal models, which is consistent with the results reported in the literature (47, 48). However, it is important to note that our model was developed and validated on a single-center retrospective dataset. While internal validation showed promising results, the generalizability of our model needs to be confirmed in multi-center, prospective studies with diverse patient populations and imaging protocols.

# Technical and clinical implications

This investigation represents the first implementation of ultrasound-based radiomics-DTL fusion for cervical cancer nodal staging, addressing 2 critical clinical needs (1): cost-effective alternatives to MRI and PET-CT in low-resource settings (4, 10), and (2) quantitative standardization of subjective ultrasound interpretation (25). The achieved diagnostic accuracy (training AUC: 0.871) positions our nomogram competitively against MRI-based models requiring specialized sequences and contrast administration (10, 49). Furthermore, the compatibility of our methodology with portable ultrasound systems enables potential deployment in screening/telemedicine contexts, which is particularly valuable in geographically dispersed populations.

However, a performance gap was observed between the training (AUC = 0.871) and testing (AUC = 0.764) cohorts. This is an expected phenomenon in machine learning, reflecting the model's adaptation to the specific patterns of the training data. It is crucial to highlight that our modeling pipeline incorporated several strategies to mitigate overfitting, including LASSO regularization and 10-fold cross-validation during feature selection. The testing AUC of 0.764, therefore, represents a more realistic estimate of the model's performance on unseen data, which remains clinically valuable and competitive with existing literature (50). Most importantly, the DCA demonstrated that the nomogram provided superior clinical net benefit across a wide range of threshold probabilities (10%–50%) in the testing set, underscoring its potential utility in clinical decision-making despite the observed drop in AUC.

# Limitations and future directions

Four principal limitations warrant consideration. First, the most significant limitation of this study is its single-center, retrospective nature. The absence of an external validation cohort from a different institution limits the assessment of the model's generalizability and robustness against variations in ultrasound equipment and operator expertise. Second, two-dimensional ROI analysis disregards volumetric heterogeneity patterns, which are increasingly being recognized as metastatic predictors. Third, the exclusion of functional ultrasound parameters (Doppler indices, elastography) omitted potentially discriminative hemodynamic data. Fourth, the monocentric training dataset (n = 294) may insufficiently represent global population diversity, requiring multicenter expansion for clinical implementation.

In the future, we will prioritize external validation in a multicenter setting to confirm the clinical translatability of our nomogram, and prospective validation efforts should focus on advancing multidimensional tumor assessment by integrating volumetric

three-dimensional sampling techniques with dynamic perfusion monitoring across treatment timelines, while concurrently establishing molecular validation frameworks through longitudinal tracking of circulating tumor DNA biomarkers.

# Conclusions

The nomogram developed in this study establishes a clinically viable framework for preoperative PLNM prediction in patients with cervical cancer, and synergistically integrates the accessibility of ultrasonography with advanced computational analytics. By achieving a diagnostic accuracy comparable to those of resource-intensive modalities through multimodal feature fusion, this approach holds particular promise for optimizing therapeutic stratification in resource-variable healthcare ecosystems.

# Data availability statement

The original contributions presented in the study are included in the article/Supplementary Material. Further inquiries can be directed to the corresponding author/s.

# **Ethics statement**

The studies involving humans were approved by Ethical permission was approved by the institutional ethics committee of the First Affiliated Hospital of Guangxi Medical University (Approval Number: 2022-KT- 077). The requirement for informed consent was waived due to the retrospective nature of the study. The studies were conducted in accordance with the local legislation and institutional requirements. Written informed consent for participation was not required from the participants or the participants' legal guardians/next of kin in accordance with the national legislation and institutional requirements.

# **Author contributions**

JWa: Conceptualization, Data curation, Formal Analysis, Investigation, Methodology, Writing – original draft, Writing – review & editing. SB: Conceptualization, Data curation, Supervision, Writing – review & editing. TH: Conceptualization, Data curation, Methodology, Writing – review & editing. YC: Investigation,

Methodology, Software, Supervision, Writing – review & editing. BJ: Project administration, Resources, Writing – review & editing. JWu: Funding acquisition, Supervision, Writing – review & editing.

# **Funding**

The author(s) declare that financial support was received for the research and/or publication of this article. The research was funded by the Key Program of Guangxi Natural Science Foundation (grant no. 2023GXNSFDA026010).

# Conflict of interest

The authors declare that the research was conducted in the absence of any commercial or financial relationships that could be construed as a potential conflict of interest.

# Generative AI statement

The author(s) declare that no Generative AI was used in the creation of this manuscript.

Any alternative text (alt text) provided alongside figures in this article has been generated by Frontiers with the support of artificial intelligence and reasonable efforts have been made to ensure accuracy, including review by the authors wherever possible. If you identify any issues, please contact us.

# Publisher's note

All claims expressed in this article are solely those of the authors and do not necessarily represent those of their affiliated organizations, or those of the publisher, the editors and the reviewers. Any product that may be evaluated in this article, or claim that may be made by its manufacturer, is not guaranteed or endorsed by the publisher.

# Supplementary material

The Supplementary Material for this article can be found online at: https://www.frontiersin.org/articles/10.3389/fonc.2025.1681029/full#supplementary-material

# References

- 1. Bray F, Laversanne M, Sung H, Ferlay J, Siegel RL, Soerjomataram I, et al. Global cancer statistics 2022: globocan estimates of incidence and mortality worldwide for 36 cancers in 185 countries. *CA: Cancer J Clin.* (2024) 74:229–63. doi: 10.3322/caac.21834
- 2. Liu S, Zhou Y, Wang C, Shen J, Zheng Y. Prediction of lymph node status in patients with early-stage cervical cancer based on radiomic features of magnetic

resonance imaging (Mri) images. BMC Med Imaging. (2023) 23:101. doi: 10.1186/s12880-023-01059-6

3. van Kol KGG, Ebisch RMF, van der Aa M, Wenzel HB, Piek JMJ, Bekkers RLM. The prognostic value of the presence of pelvic and/or para-aortic lymph node metastases in cervical cancer patients; the influence of the new figo classification (Stage iiic). *Gynecol Oncol.* (2023) 171:9–14. doi: 10.1016/j.ygyno.2023.01.023

- 4. Abu-Rustum NR, Yashar CM, Arend R, Barber E, Bradley K, Brooks R, et al. Nccn guidelines<sup>®</sup> Insights: cervical cancer, version 1.2024. *J Natl Compr Canc Netw.* (2023) 21:1224–33. doi: 10.6004/jnccn.2023.0062
- 5. Maeda M, Mabuchi S, Sakata M, Deguchi S, Kakubari R, Matsuzaki S, et al. Significance of tumor size and number of positive nodes in patients with figo 2018 stage iiic1 cervical cancer. *Jpn J Clin Oncol.* (2024) 54:146–52. doi: 10.1093/jjco/hyad141
- 6. Bhatla N, Denny L. Figo cancer report 2018. Int J Gynaecol Obstet. (2018) 143 Suppl 2:2–3. doi: 10.1002/ijgo.12608
- 7. Cibula D, Pötter R, Planchamp F, Avall-Lundqvist E, Fischerova D, Haie Meder C, et al. The european society of gynaecological oncology/european society for radiotherapy and oncology/european society of pathology guidelines for the management of patients with cervical cancer. *Radiother Oncol.* (2018) 127:404–16. doi: 10.1016/j.radonc.2018.03.003
- 8. Mazzola R, Ricchetti F, Fiorentino A, Levra NG, Fersino S, Di Paola G, et al. Weekly cisplatin and volumetric-modulated arc therapy with simultaneous integrated boost for radical treatment of advanced cervical cancer in elderly patients: feasibility and clinical preliminary results. *Technol Cancer Res Treat.* (2017) 16:310–5. doi: 10.1177/1533034616655055
- 9. Obrzut B, Semczuk A, Naróg M, Obrzut M, Król P. Prognostic parameters for patients with cervical cancer figo stages ia2-iib: A long-term follow-up. *Oncology*. (2017) 93:106–14. doi: 10.1159/000471766
- 10. Li L, Zhang J, Zhe X, Tang M, Zhang X, Lei X, et al. A meta-analysis of mri-based radiomic features for predicting lymph node metastasis in patients with cervical cancer. *Eur J Radiol.* (2022) 151:110243. doi: 10.1016/j.ejrad.2022.110243
- 11. Zou Y, Zhu S, Kong Y, Feng C, Wang R, Lei L, et al. Precision matters: the value of pet/ct and pet/mri in the clinical management of cervical cancer. *Strahlenther Onkol.* (2024) 201:507-518. doi: 10.1007/s00066-024-02294-8
- 12. Lee JH, Jeong YK, Park KB, Park JK, Jeong AK, Hwang JC. Operator-dependent techniques for graded compression sonography to detect the appendix and diagnose acute appendicitis.  $AJR\ Am\ J\ Roentgenol.\ (2005)\ 184:91-7.\ doi:\ 10.2214/\ ajr.184.1.01840091$
- 13. Lécuru F, Mathevet P, Querleu D, Leblanc E, Morice P, Daraï E, et al. Bilateral negative sentinel nodes accurately predict absence of lymph node metastasis in early cervical cancer: results of the senticol study. *J Clin Oncol.* (2011) 29:1686–91. doi: 10.1200/jco.2010.32.0432
- 14. Song XY, Yuan XM, Chen WJ, Pan T, Xie SD, Qin C, et al. Different criteria for radioactive sentinel lymph nodes has different impact on sentinel node biopsy in breast cancer patients. *J Surg Oncol.* (2007) 95:635–9. doi: 10.1002/jso.20757
- 15. Kummar S, Lu R. Using radiomics in cancer management. *JCO Precis Oncol.* (2024) 8:e2400155. doi: 10.1200/po.24.00155
- 16. Xie CY, Pang CL, Chan B, Wong EY, Dou Q, Vardhanabhuti V. Machine learning and radiomics applications in esophageal cancers using non-invasive imaging methods-a critical review of literature. *Cancers*. (2021) 13:2469. doi: 10.3390/cancers13102469
- 17. Wang Y, Gao J, Yin Z, Wen Y, Sun M, Han R. Differentiation of benign and Malignant parotid gland tumors based on the fusion of radiomics and deep learning features on ultrasound images. *Front Oncol.* (2024) 14:1384105. doi: 10.3389/fonc.2024.1384105
- 18. Lu G, Tian R, Yang W, Liu R, Liu D, Xiang Z, et al. Deep learning radiomics based on multimodal imaging for distinguishing benign and Malignant breast tumours. *Front Med (Lausanne)*. (2024) 11:1402967. doi: 10.3389/fmed.2024.1402967
- 19. Voutouri C, Mpekris F, Panagi M, Krolak C, Michael C, Martin JD, et al. Ultrasound stiffness and perfusion markers correlate with tumor volume responses to immunotherapy. *Acta Biomater*. (2023) 167:121–34. doi: 10.1016/j.actbio.2023.06.007
- 20. Han X, Qu J, Chui ML, Gunda ST, Chen Z, Qin J, et al. Artificial intelligence performance in ultrasound-based lymph node diagnosis: A systematic review and meta-analysis. *BMC Cancer*. (2025) 25:73. doi: 10.1186/s12885-025-13447-y
- 21. Miller KM, Liu C, Zhou Q, Iasonos A, Baser R, Ramesh B, et al. Relevant-C Study: Patient-Reported Prevalence of Lower Extremity Lymphedema after Sentinel Lymph Node Mapping Vs Lymphadenectomy after Surgery for Early-Stage Cervical Cancer. *Int J Gynecol Cancer*. (2025) 35:100063. doi: 10.1016/j.ijgc.2024.100063
- 22. Wedin M, Stålberg KG, Ottander U, Åkesson Å, Lindahl G, Wodlin NB, et al. Risk factors for lymph ascites after surgery for endometrial cancer and impact on lymphedema of the legs. A prospective longitudinal swedish multicenter study. *Acta obstetricia gynecologica Scandinavica*. (2025) 104:976-987. doi: 10.1111/aogs.15077
- 23. Cibula D, Raspollini MR, Planchamp F, Centeno C, Chargari C, Felix A, et al. Esgo/estro/esp guidelines for the management of patients with cervical cancer update 2023. *Int J Gynecol Cancer*. (2023) 33:649–66. doi: 10.1136/ijgc-2023-004429
- 24. Fischerova D, Frühauf F, Burgetova A, Haldorsen IS, Gatti E, Cibula D. The role of imaging in cervical cancer staging: esgo/estro/esp guidelines (Update 2023). *Cancers*. (2024) 16:775. doi: 10.3390/cancers16040775
- 25. Tong Y, Li J, Huang Y, Zhou J, Liu T, Guo Y, et al. Ultrasound-based radiomic nomogram for predicting lateral cervical lymph node metastasis in papillary thyroid carcinoma. *Acad Radiol.* (2021) 28:1675–84. doi: 10.1016/j.acra.2020.07.017
- 26. Zhang D, Yang F, Hou W, Wang Y, Mu J, Wang H, et al. Ultrasonic radiomics in predicting pathologic type for thyroid cancer: A preliminary study using radiomics features for predicting medullary thyroid carcinoma. *Front Endocrinol (Lausanne)*. (2025) 16:1428888. doi: 10.3389/fendo.2025.1428888

- 27. Zhou C, Zhou J, Lv Y, Batuer M, Huang J, Zhong J, et al. The impact of the novel covbat harmonization method on enhancing radiomics feature stability and machine learning model performance: A multi-center, multi-device study. *Eur J Radiol.* (2025) 184:111956. doi: 10.1016/j.ejrad.2025.111956
- 28. Zhang YC, Li M, Jin YM, Xu JX, Huang CC, Song B. Radiomics for differentiating tumor deposits from lymph node metastasis in rectal cancer. *World J Gastroenterol.* (2022) 28:3960–70. doi: 10.3748/wjg.v28.i29.3960
- 29. Gao X, Ma T, Cui J, Zhang Y, Wang L, Li H, et al. A ct-based radiomics model for prediction of lymph node metastasis in early stage gastric cancer. *Acad Radiol.* (2021) 28:e155–e64. doi: 10.1016/j.acra.2020.03.045
- 30. LeCun Y, Bengio Y, Hinton G. Deep learning. Nature. (2015) 521:436–44. doi: 10.1038/nature14539
- 31. Bo L, Zhang Z, Jiang Z, Yang C, Huang P, Chen T, et al. Differentiation of brain abscess from cystic glioma using conventional mri based on deep transfer learning features and hand-crafted radiomics features. Front Med (Lausanne). (2021) 8:748144. doi: 10.3389/fmed.2021.748144
- 32. Feng B, Huang L, Liu Y, Chen Y, Zhou H, Yu T, et al. A transfer learning radiomics nomogram for preoperative prediction of borrmann type iv gastric cancer from primary gastric lymphoma. *Front Oncol.* (2021) 11:802205. doi: 10.3389/fonc.2021.802205
- 33. Sun Y, Lu Z, Yang H, Jiang P, Zhang Z, Liu J, et al. Prediction of lateral lymph node metastasis in rectal cancer patients based on mri using clinical, deep transfer learning, radiomic, and fusion models. *Front Oncol.* (2024) 14:1433190. doi: 10.3389/fonc.2024.1433190
- 34. Zeng Q, Li H, Zhu Y, Feng Z, Shu X, Wu A, et al. Development and validation of a predictive model combining clinical, radiomics, and deep transfer learning features for lymph node metastasis in early gastric cancer. *Front Med (Lausanne)*. (2022) 9:986437. doi: 10.3389/fmed.2022.986437
- 35. Hsu ST, Su YJ, Hung CH, Chen MJ, Lu CH, Kuo CE. Automatic ovarian tumors recognition system based on ensemble convolutional neural network with ultrasound imaging. *BMC Med Inform Decis Mak.* (2022) 22:298. doi: 10.1186/s12911-022-02047-6
- 36. Gong J, Zhang W, Huang W, Liao Y, Yin Y, Shi M, et al. Ct-based radiomics nomogram may predict local recurrence-free survival in esophageal cancer patients receiving definitive chemoradiation or radiotherapy: A multicenter study. *Radiother Oncol.* (2022) 174:8–15. doi: 10.1016/j.radonc.2022.06.010
- 37. Song E, Long J, Ma G, Liu H, Hung CC, Jin R, et al. Prostate lesion segmentation based on a 3d end-to-end convolution neural network with deep multi-scale attention. *Magn Reson Imaging.* (2023) 99:98–109. doi: 10.1016/j.mri.2023.01.015
- 38. Liu J, Wang Z, Shao H, Qu D, Liu J, Yao L. Improving ct detection sensitivity for nodal metastases in oesophageal cancer with combination of smaller size and lymph node axial ratio. *Eur Radiol.* (2018) 28:188–95. doi: 10.1007/s00330-017-4935-4
- 39. Wan L, Hu J, Chen S, Zhao R, Peng W, Liu Y, et al. Prediction of lymph node metastasis in stage T1–2 rectal cancers with MRI-based deep learning. *Eur Radiol.* (2023) 33:3638–46. doi: 10.1007/s00330-023-09450-1
- 40. Cui XW, Li KN, Yi AJ, Wang B, Wei Q, Wu GG, et al. Ultrasound elastography. Endosc Ultrasound. (2022) 11:252–74. doi: 10.4103/EUS-D-21-00151
- 41. Liu Y, Huang Y, Han J, Wang J, Li F, Zhou J. Association between shear wave elastography of virtual touch tissue imaging quantification parameters and the ki-67 proliferation status in luminal-type breast cancer. *J Ultrasound Med.* (2019) 38:73–80. doi: 10.1002/jum.14663
- 42. Eisenbrey JR, Gabriel H, Savsani E, Lyshchik A. Contrast-enhanced ultrasound (CEUS) in HCC diagnosis and assessment of tumor response to locoregional therapies. *Abdom Radiol (NY)*. (2021) 46:3579–95. doi: 10.1007/s00261-021-03059-y
- 43. Chen XL, Chen GW, Xu GH, Ren J, Li ZL, Pu H, et al. Tumor size at magnetic resonance imaging association with lymph node metastasis and lymphovascular space invasion in resectable cervical cancer: A multicenter evaluation of surgical specimens. *Int J Gynecol Cancer*. (2018) 28:1545–52. doi: 10.1097/igc.0000000000001327
- 44. Wang W, Liu X, Meng Q, Zhang F, Hu K. Nomogram for predicting para-aortic lymph node metastases in patients with cervical cancer. *Arch Gynecol Obstet.* (2018) 298:381–8. doi: 10.1007/s00404-018-4829-y
- 45. Cao L, Kong W, Li J, Song D, Jin B, Liu T, et al. Analysis of lymph node metastasis and risk factors in 975 patients with figo 2009 stage ia-iia cervical cancer. *Gynecol Obstet Invest.* (2023) 88:30–6. doi: 10.1159/000527712
- 46. Lang E, Bissinger R, Qadri SM, Lang F. Suicidal death of erythrocytes in cancer and its chemotherapy: A potential target in the treatment of tumor-associated anemia. *Int J Cancer.* (2017) 141:1522–8. doi: 10.1002/ijc.30800
- 47. Song D, Yang F, Zhang Y, Guo Y, Qu Y, Zhang X, et al. Dynamic contrast-enhanced mri radiomics nomogram for predicting axillary lymph node metastasis in breast cancer. *Cancer Imaging*. (2022) 22:17. doi: 10.1186/s40644-022-00450-w
- 48. Wang D, Hu Y, Zhan C, Zhang Q, Wu Y, Ai T. A nomogram based on radiomics signature and deep-learning signature for preoperative prediction of axillary lymph node metastasis in breast cancer. *Front Oncol.* (2022) 12:940655. doi: 10.3389/fonc.2022.940655
- 49. Deng X, Liu M, Sun J, Li M, Liu D, Li L, et al. Feasibility of mri-based radiomics features for predicting lymph node metastases and vegf expression in cervical cancer. *Eur J Radiol.* (2021) 134:109429. doi: 10.1016/j.ejrad.2020.109429
- 50. Wang T, Li YY, Ma NN, Wang PA, Zhang B. A MRI radiomics-based model for prediction of pelvic lymph node metastasis in cervical cancer. *World J Surg Oncol.* (2024) 22:55. doi: 10.1186/s12957-024-03333-5